DOT/FAA/TC-19/4

Federal Aviation Administration
William J. Hughes Technical Center
Aviation Research Division
Atlantic City International Airport
New Jersey 08405

Cyclic Plate Testing of Reinforced Airport Pavements – Phase II: Geosynthetics

February 2019

Final Report

U.S. Department of Transportation
Federal Aviation Administration

NOTICE

Technical Report Documentation Page

1. Report No.	2. Government Accession No.	3. Recipient's Catalog No.
DOT/FAA/TC-19/4		

4. Title and Subtitle	5. Report Date
CYCLIC PLATE TESTING OF REINFORCED AIRPORT PAVEMENTS – PHASE II: GEOSYNTHETICS	February 2019
	6. Performing Organization Code USACE-ERDC
7. Author(s) William J. Robinson and Gregory J. Norwood	8. Performing Organization Report No.
9. Performing Organization Name and Address U.S. Army Engineer Research and Development Center Geotechnical and Structures Laboratory 3909 Halls Ferry Road Vicksburg, MS 39180-6199	10. Work Unit No. (TRAIS) 11. Contract or Grant No.
12. Sponsoring Agency Name and Address U.S. Department of Transportation Federal Aviation Administration Air Traffic Organization Operations Planning Office of Aviation Research and Development Washington, DC 20591	13. Type of Report and Period Covered Final Report 14. Sponsoring Agency Code AAS-100

15. Supplementary Notes

The Federal Aviation Administration Aviation Research Division COR was Mr. Benjamin J. Mahaffay.

16. Abstract

Although geosynthetics have been used in highway pavement applications for years, knowledge regarding the use of geosynthetics in airfield pavements is limited. This study evaluated the effect of incorporating geosynthetics in pavement structures subjected to heavy aircraft loadings. Representative flexible pavement structures were constructed in a laboratory-scale testing facility and subjected to simulated aircraft load via a 12-in.-diameter plate. A total of seven representative airfield pavement structures were evaluated, four of which included geosynthetic reinforcement at the subgrade/subbase material interface. Each pavement structure was instrumented with earth pressure cells (EPCs) to measure layer response. Permanent deformation data were collected, and traffic benefit ratios (TBRs) were calculated to determine relative improvement when compared to an unreinforced pavement structure. Tested using medium-scale cyclic plate loading, it was observed that inclusion of some geosynthetics in airfield pavements displayed a performance benefit evidenced by increased cycles-to-failure and a TBR greater than one when compared to a similar unreinforced pavement. Results suggest that placing a geosynthetic deeper in a relatively thick airfield pavement may reduce the potential performance benefit.

17. Key Words	18. Distribution Statement
Cyclic plate testing, Pavement design, Traffic benefit ratio, Geosynthetic, Reinforcement, Flexible pavement	This document is available to the U.S. public through the National Technical Information Service (NTIS), Springfield, Virginia 22161. This document is also available from the Federal Aviation Administration William J. Hughes Technical Center at actlibrary.tc.faa.gov.

19. Security Classif. (of this report)	20. Security Classif. (of this page)	21. No. of Pages	22. Price
Unclassified	Unclassified	46	

TABLE OF CONTENTS

LIST OF FIGURES

LIST OF TABLES

LIST OF ACRONYMS

AASHTO	American Association of State Highway and Transportation Officials
ASTM	American Society for Testing and Materials
C_c	Coefficient of curvature
C_u	Coefficient of uniformity
CBR	California bearing ratio
CH	High-plasticity clay
CMD	Cross-machine direction
EPC	Earth pressure cell
ERDC	Engineer Research and Development Center
FAA	Federal Aviation Administration
G_{mm}	Theoretical maximum specific gravity
GW-GM	Well-graded gravel with salt and sand
HMA	Hot-mix asphalt
kN/m	Kilonewton meter
LL	Liquid limit
LVDT	Linear variable displacement transducer
MD	Machine direction
pcf	Pounds per cubic foot
PI	Plasticity index
PL	Plastic limit
psi	Pounds per square inch
SHRP	Strategic Highway Research Program
SW	Well-graded sand
TBR	Traffic benefit ratio
U.S.	United States
USCS	Unified Soil Classification System

EXECUTIVE SUMMARY

Although geosynthetics have been used in highway pavement applications for years, knowledge regarding the use of geosynthetics in airfield pavements is limited. This study was performed to evaluate the effect of incorporating geosynthetics in pavement structures subjected to heavy aircraft loadings. Representative flexible pavement structures were constructed in a laboratory-scale testing facility, and simulated aircraft load was applied via a 12-in.-diameter plate. A total of seven representative airfield pavement structures were evaluated, four of which included geosynthetic reinforcement at the subgrade/subbase interface. Each pavement structure was instrumented with earth pressure cells (EPCs) and linear variable displacement transducers (LVDT) to measure pavement response parameters. Permanent deformation data were collected, and traffic benefit ratios (TBRs) were calculated to determine relative improvement when compared to an unreinforced pavement structure. Comparisons were made to previous test items (Phase I) incorporating geosynthetics at the subbase/base interface to evaluate the effect of placement location within the pavement structure.

The following are the main findings from this study.

- Tested using medium-scale cyclic plate loading, the inclusion of geosynthetics in airfield pavements display a performance benefit evidenced by increased cycles-to-failure and a TBR greater than one when compared to a similar unreinforced pavement.

- Data suggest that placing a geosynthetic deeper in a relatively thick airfield pavement may reduce the potential performance benefit.

- Some level of permanent deformation may be required to engage the reinforcing benefit of geotextiles as suggested by higher TBR at higher deformation values.

- The geosynthetics did not provide the same performance benefit as incorporating a subbase with 50+ California bearing ratio (CBR) in the pavement system.

- Changing subbase material type and consequently CBR from approximately 20 to greater than 50 resulted in significant performance improvement.

1. INTRODUCTION.

Although geosynthetics have been used in highway pavement applications for years, it is not until recently that pavement design engineers proposed using geosynthetics in airfield pavement design. The Federal Aviation Administration (FAA) is interested in determining the merit of using geosynthetics as a structural element in flexible airfield pavement design. Traditionally, geosynthetic pavement systems tests were performed in the form of construction and accelerated trafficking of full-scale pavement test sections. These tests tend to be costly and time-consuming in terms of both construction and testing. Pavement structures constructed in a medium-scale laboratory box apparatus provide an opportunity to quantify benefits of geosynthetic reinforcement at a reduced cost compared to full-scale traffic testing.

1.1 ISSUES.

Numerous research studies were undertaken to determine performance improvement gained from incorporating geosynthetics in flexible pavement systems. A majority of studies focused on relatively thin pavement structures subjected to highway loads. Airfield pavements can be substantially thicker and include multiple aggregate layers when compared to highway pavements. Data are needed to quantify pavement performance and identify optimal placement location of geosynthetics within an airfield pavement structure.

1.2 OBJECTIVES.

The technical objective of this study was to conduct medium-scale laboratory testing of representative flexible airfield pavements including different types of geosynthetic reinforcement. These different products and methods were compared to one another, as well as to an unreinforced control test, based on pavement performance under simulated aircraft loadings. Pavement performance was measured in terms of permanent surface deformation, which was used to calculate a traffic benefit ratio (TBR) for each product tested. The American Association of State Highway Transportation Officials (AASHTO) R 50-09 defines TBRs as the ratio of the number of load cycles of a reinforced pavement structure to reach a defined failure state to the number of load cycles of an identical unreinforced pavement structure [1]. Results were combined with previous testing (Phase I) conducted by the United States (U.S.) Army Engineer Research and Development Center (ERDC) to compare the influence of geosynthetic placement location.

The primary objective of this project was to quantify the performance of a representative geosynthetic-reinforced flexible pavement under simulated heavy aircraft loading. The approach was to construct medium-scale laboratory tests, each with a unique geosynthetic, and observe pavement performance under cyclic loading. Instrumentation response data in each pavement section were also obtained for comparison of pavement response parameters.

2. TEST PLAN AND LAYOUT.

The test series consisted of seven different test items constructed in a 6- by 6- by 6-ft steel box used as a containment facility for medium-scale laboratory pavement structures. The box was composed of 1-in.-thick steel plates reinforced with 1/4-in.-thick, 6-in.-square structural steel

tubing along the bottom and three sides of the box. The front of the box consisted of removable 1/4-in.-thick, 6-in.-square structural steel tubing to facilitate construction of the pavement test section. Figure 1 shows the medium-scale laboratory test box with the front removed.

Figure 1. Medium-Scale Laboratory Test Box (Front Removed)

Subgrade soils were constructed with a nominal 28 in. of high-plasticity clay (CH) placed to achieve a target California bearing ratio (CBR) value of 3% and 2%. The CBR percentage values were selected to provide test sections with low subgrade strength where pavement structure reinforcement is a significant consideration. The subgrade was overlain with a 12-in.-thick subbase course consisting of granular material meeting FAA P-154 specifications and provided by the FAA for test item 1 and coarse sand meeting FAA P-154 specifications for test Items 2 through 7. A 7-in.-thick crushed limestone base course was placed over the subbase. The surface layer consisted of a 5-in.-thick hot-mix asphalt (HMA) slab. The overall thickness of each test section was approximately 52 in. Test item 1 was an unreinforced control section with the FAA-provided granular subbase material. Because the material demonstrated unusual strength improvement for a subbase, test item 1 was the only one that included the FAA-provided granular subbase material. Thus, test items 2 through 7 included a sand subbase that met the FAA subbase criteria but did not demonstrate unusual strength properties. Test item 2 was constructed using Tensar® BX1200 geogrid at the subbase-subgrade interface. Test item 3 was constructed using Tensar TriAx® TX140 geogrid at the subbase-subgrade interface. Test item 4 was constructed with HUESKER® Fornit® 40/40-25T geogrid at the subbase-subgrade interface, and test item 5 was constructed with TenCate Mirafi® RS580*i* geotextile at the subbase-subgrade interface. Test items 6 and 7 consisted of unreinforced control sections with a coarse sand subbase constructed over a 3 CBR and 2 CBR clay subgrade, respectively. Figure 2 shows a typical cross-section of the seven test items.

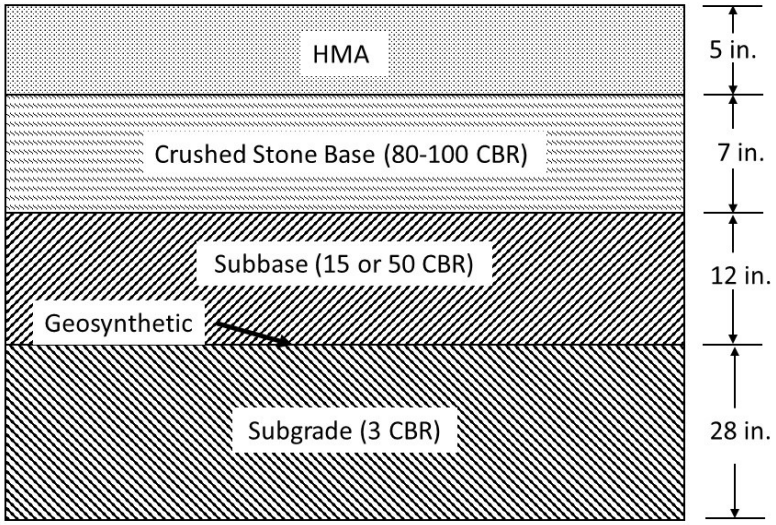

Figure 2. Typical Test Item Cross-Section

The test items contained a suite of instrumentation consisting of earth pressure cells (EPCs), moisture probes, pore-water pressure transducers, and linear variable displacement transducers (LVDTs), which are described in detail in section 4.

Loading was applied to each test item using a 50,000-lb Gilmore hydraulic actuator controlled with a MTS Systems® control system. A 28,800-lb applied load was transmitted to the pavement by a 12-in.-diameter plate yielding a 254-lb per square inch (psi) simulated aircraft contact pressure. This contact area and pressure simulated a Boeing B-777 aircraft. Load response data from the EPCs and LVDTs were continuously collected at a frequency of 300 Hz. For each test item, the failure criteria were 2 in. of permanent surface deformation measured at the load plate.

Loading was applied sinusoidally, and each pulse had a total duration of 1.2 seconds. Load was applied for a 0.3 second duration followed by a 0.9 second rest period. During the rest period, a 100-lb surcharge load was maintained to ensure the plate remained in contact with the pavement surface while allowing elastic rebound of the pavement.

3. MATERIALS.

3.1 SUBGRADE.

Each test item used a locally sourced CH to construct the nominal 28-in.-thick subgrade. A particle size analysis, shown in figure 3, indicated that the material consisted of 98.5% fines passing the No. 200 sieve. The soil had a liquid limit (LL) of 84%, a plastic limit (PL) of 29%, and a plasticity index (PI) of 55%, as determined by American Society for Testing and Materials (ASTM) D4318-17e1 [2]. According to the Unified Soil Classification System (USCS) [3], the soil was classified as a CH and an A-7-6 according to the AASHTO classification system [4].

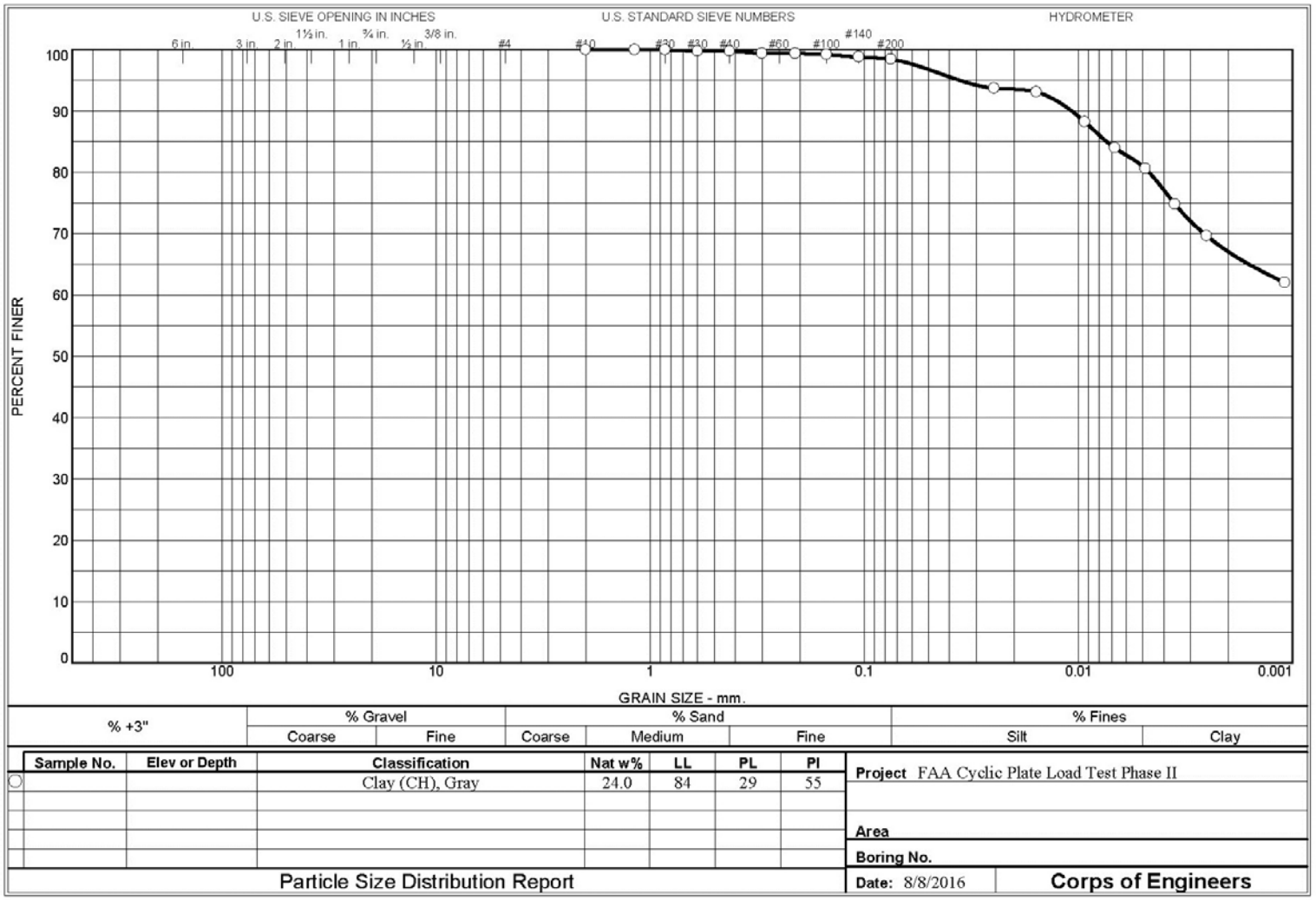

NAT W% = Natural moisture content

Figure 3. The CH Subgrade Particle Size Distribution

Modified proctor compaction tests (ASTM D1557-12e1) [5] were performed to determine the relationship between moisture content and dry density. The maximum dry density for the CH soil was found to be 102.4 lb per cubic foot (pcf) at an optimum moisture content of 22.8%. Graphical results of the moisture-density relationship test are shown in figure 4.

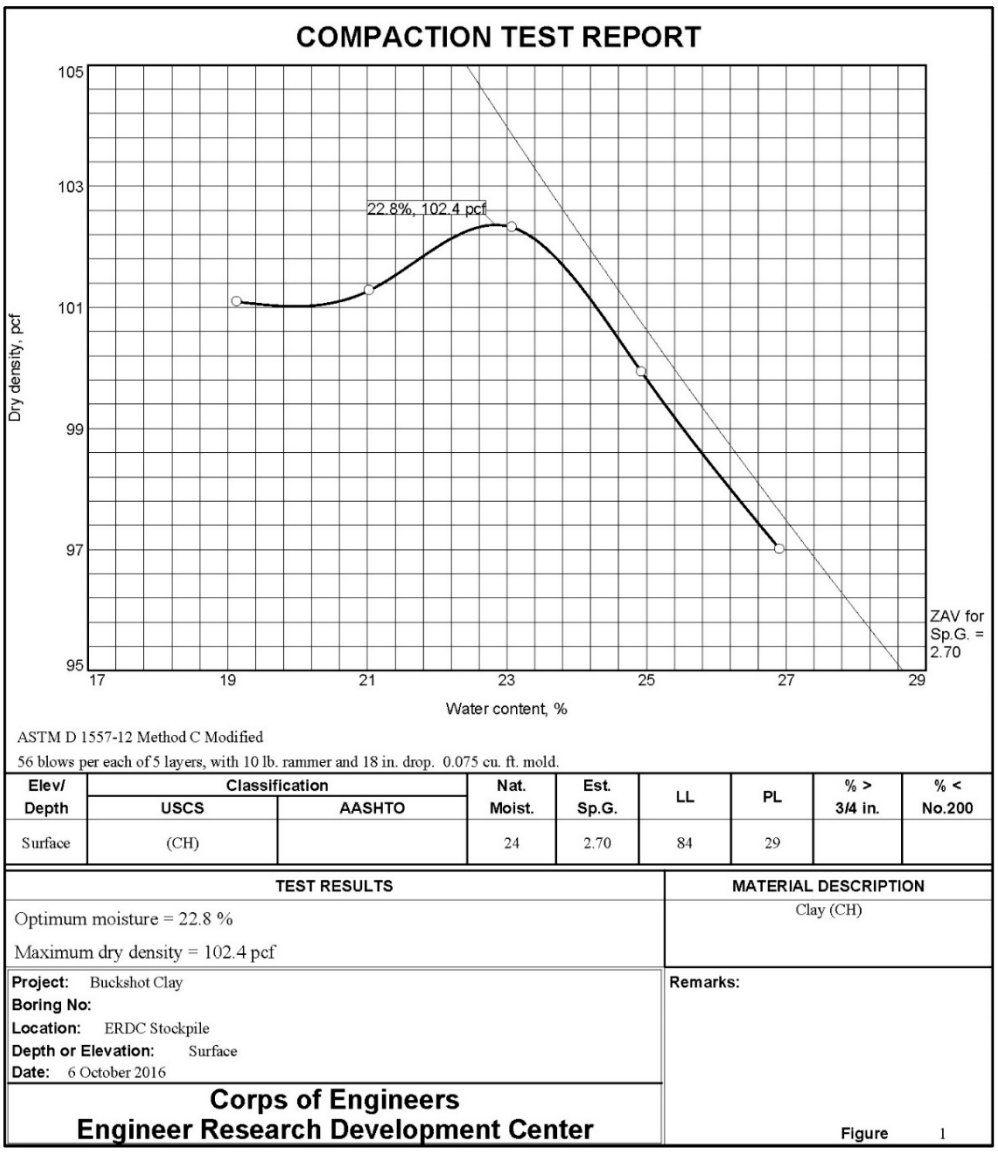

ZAV = Zero air voids
Sp. G = Specific gravity
Nat. Moist. = Natural moisture content

Figure 4. Subgrade Moisture-Density Relationship

To determine the in-place moisture content for the CH subgrade at the targeted 3 CBR, a variety of laboratory CBR tests (ASTM D1883-16) [6] were performed. These tests were conducted at moisture contents ranging from approximately 17% to 40%. A target in-place moisture content

of 38% was selected for the CH subgrade based upon the relationship between moisture content and CBR, as shown in figure 5.

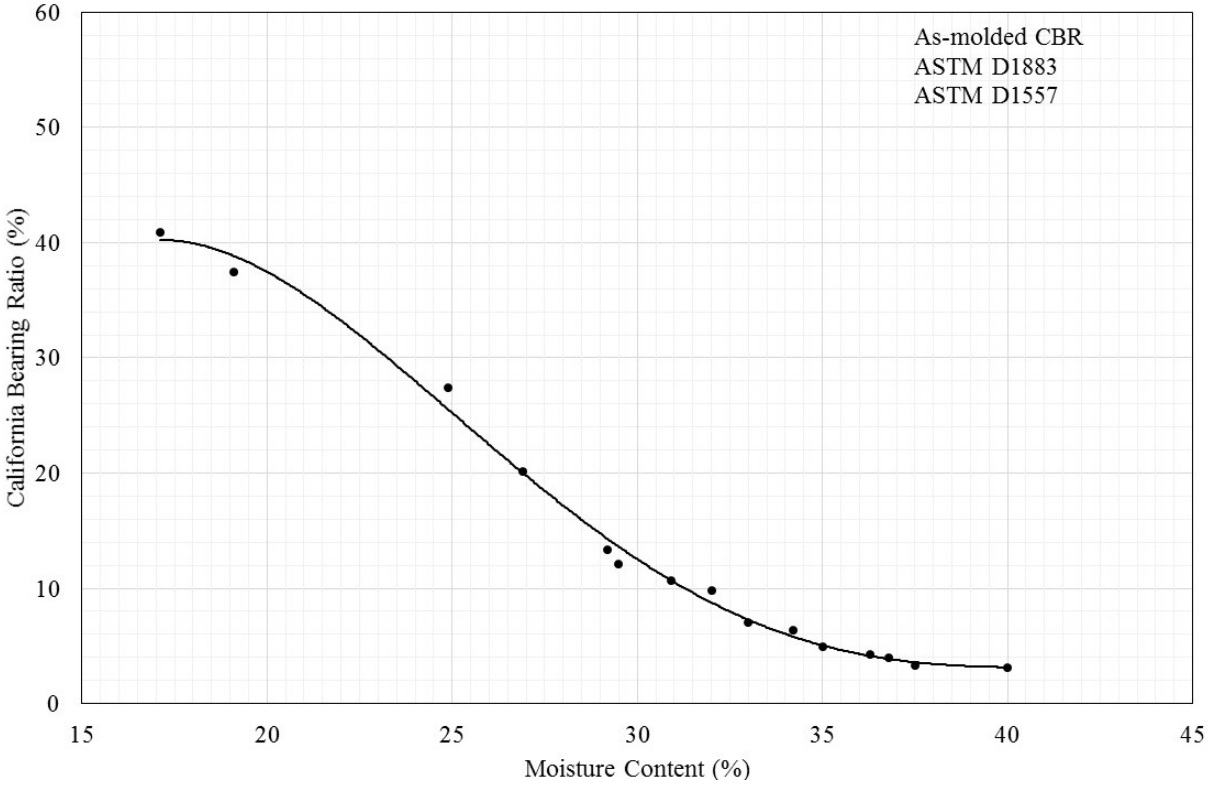

Figure 5. Subgrade CBR and Moisture Content Relationship

3.2 SUBBASE COURSE.

The subbase for Item 1 were crushed stone screenings provided by the FAA William J. Hughes Technical Center and met the requirements of FAA P-154. The gradation for the FAA P-154 is shown in table 1. ASTM D2487 [3] was used to determine that the subbase course was comprised of 6% gravel, 94% sand, and 0% nonplastic fines passing the No. 200 sieve. The coefficient of curvature (C_c) was calculated as 1.2, and the coefficient of uniformity (C_u) was 7.9. The FAA P-154 subbase was classified as a well-graded sand (SW) according to the USCS [3] and an A-1-b according to the AASHTO procedure [4]. Modified proctor compaction tests (figure 6) [5] were performed in accordance with ASTM D1557-12e1 Method B Modified [5] resulting in maximum dry density of 136.8 pcf at an optimum moisture content of 8.1%.

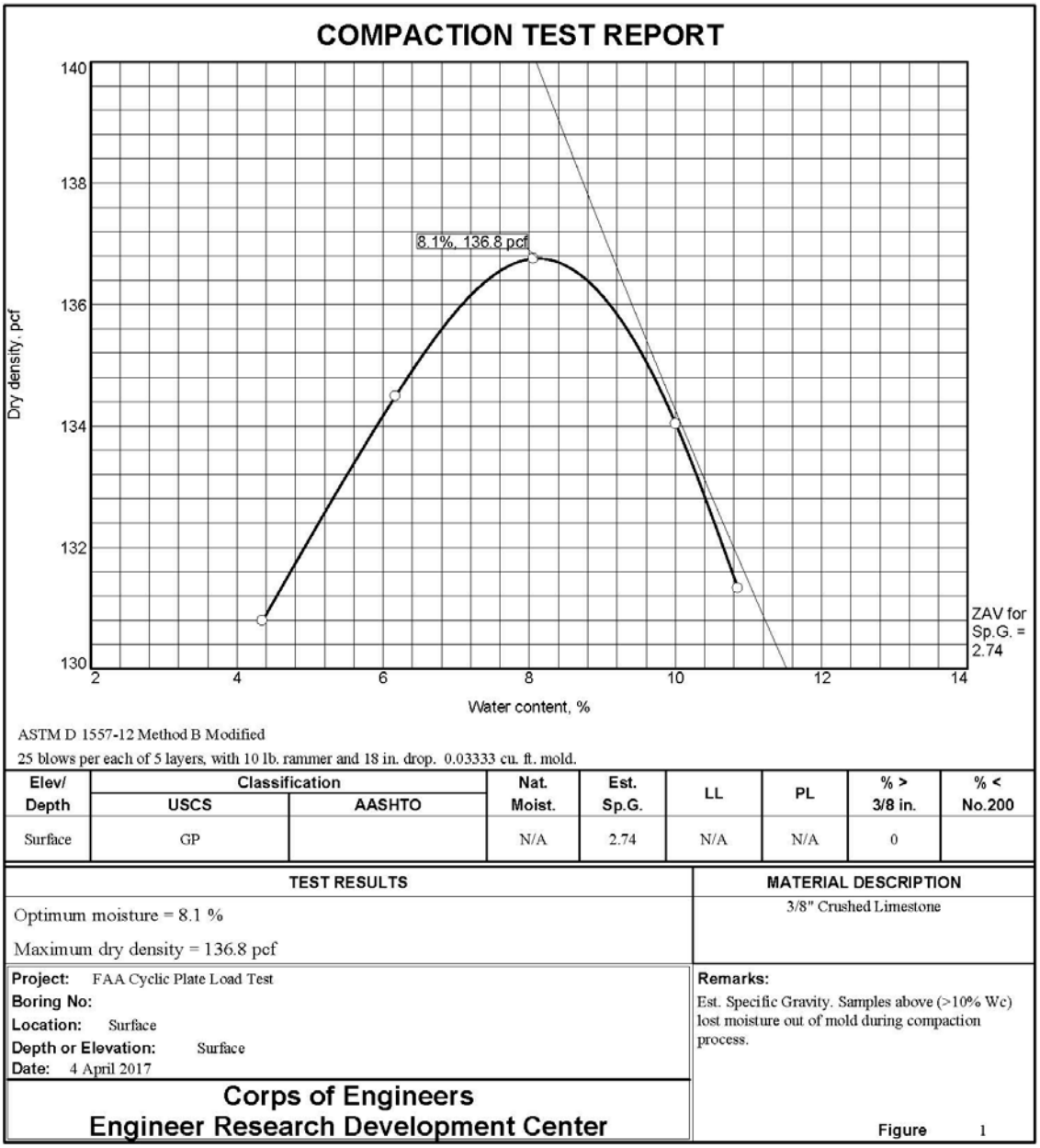

Figure 6. The FAA-Provided P-154 Subbase Course Moisture-Density Relationship

Items 2 through 7 used a locally available coarse sand subbase, which was provided by the U.S. Army Corps of Engineers ERDC and met FAA P-154 requirements. This subbase did not have intrinsic strength properties and was considered representative of an average to poor quality subbase. The gradation for the coarse sand is shown in table 1. ASTM procedure D2487 [3] was used to determine that the subbase course was comprised of 1% gravel, 99% sand, and 0% nonplastic fines passing the No. 200 sieve. The C_c was calculated as 0.7, and the C_u was 6.0. The coarse sand subbase was classified as SW according to the USCS [3] and an A-3 according to the AASHTO procedure [4].

Table 1. Subbase Particle Size Distribution

Sieve Size	FAA P-154 (Item 1)	ERDC P-154 (Items 2-7)
3 in. (75.0 mm)	100	100
3/4 in. (19.0 mm)	100	100
3/8 in. (9.5 mm)	98	100
No. 4 (4.75 mm)	94	99
No. 10 (2.00 mm)	62	91
No. 40 (0.425 mm)	15	51
No. 200 (0.075 mm)	0.5	0.1

3.3 BASE COURSE.

Locally available crushed limestone was used to construct the flexible aggregate base course. The gradation for the crushed limestone is shown in figure 7. ASTM D2487 [3] was used to determine that the base course was comprised of 71.5% gravel, 23.3% sand, and 5.2% nonplastic fines passing the No. 200 sieve. The C_c was calculated as 2.71, and the C_u was 21.16. The crushed limestone aggregate base was classified as a well-graded gravel with silt and sand (GW-GM) according to the USCS [3] and an A-1-a according to the AASHTO procedure [3]. Modified proctor compaction tests (figure 8) [5] were performed in accordance with ASTM D1557-12e1 Method C Modified [5]. The maximum dry density was 146.7 pcf at an optimum moisture content of 5.9%.

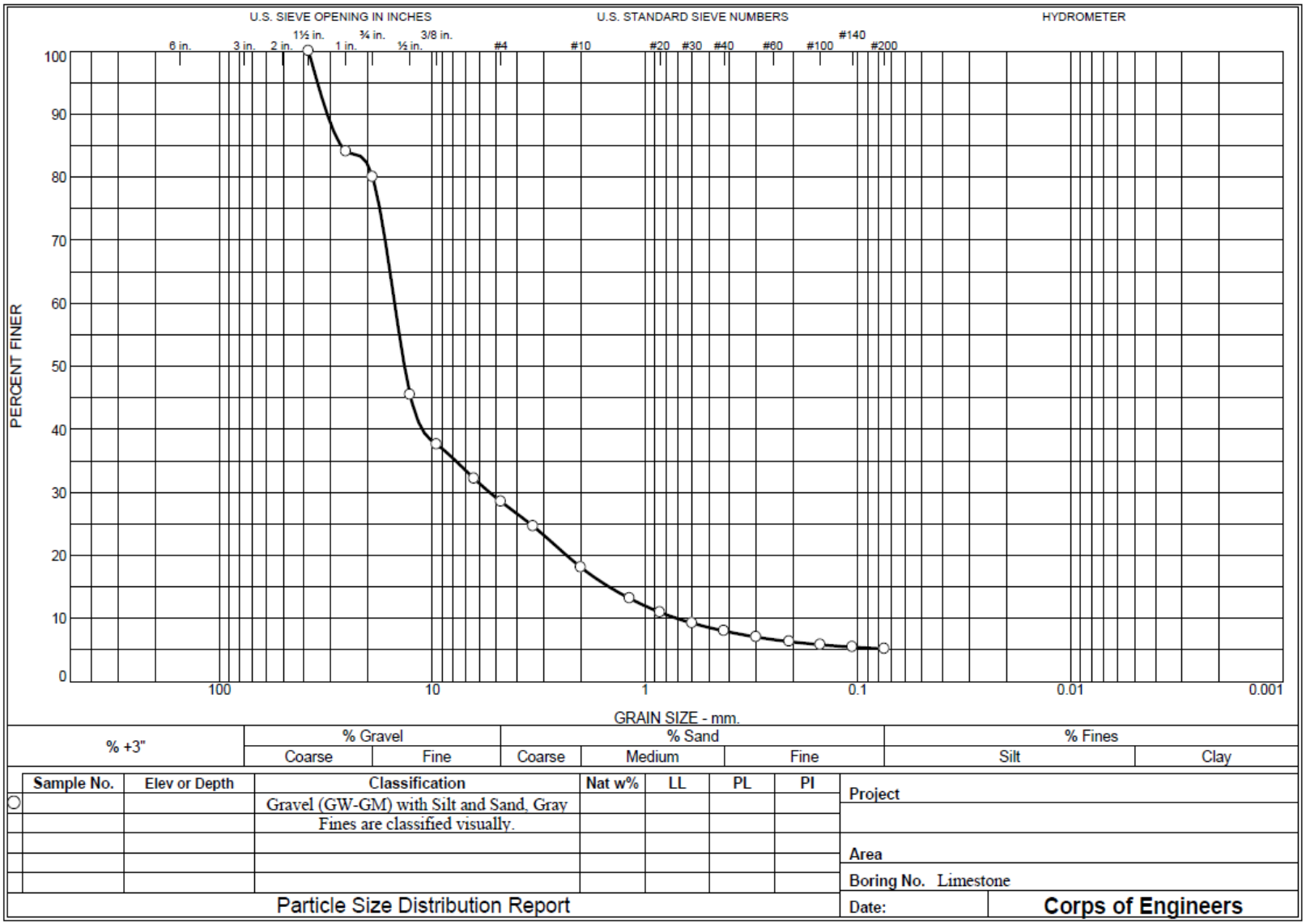

Figure 7. Crushed Limestone Particle Size Analysis

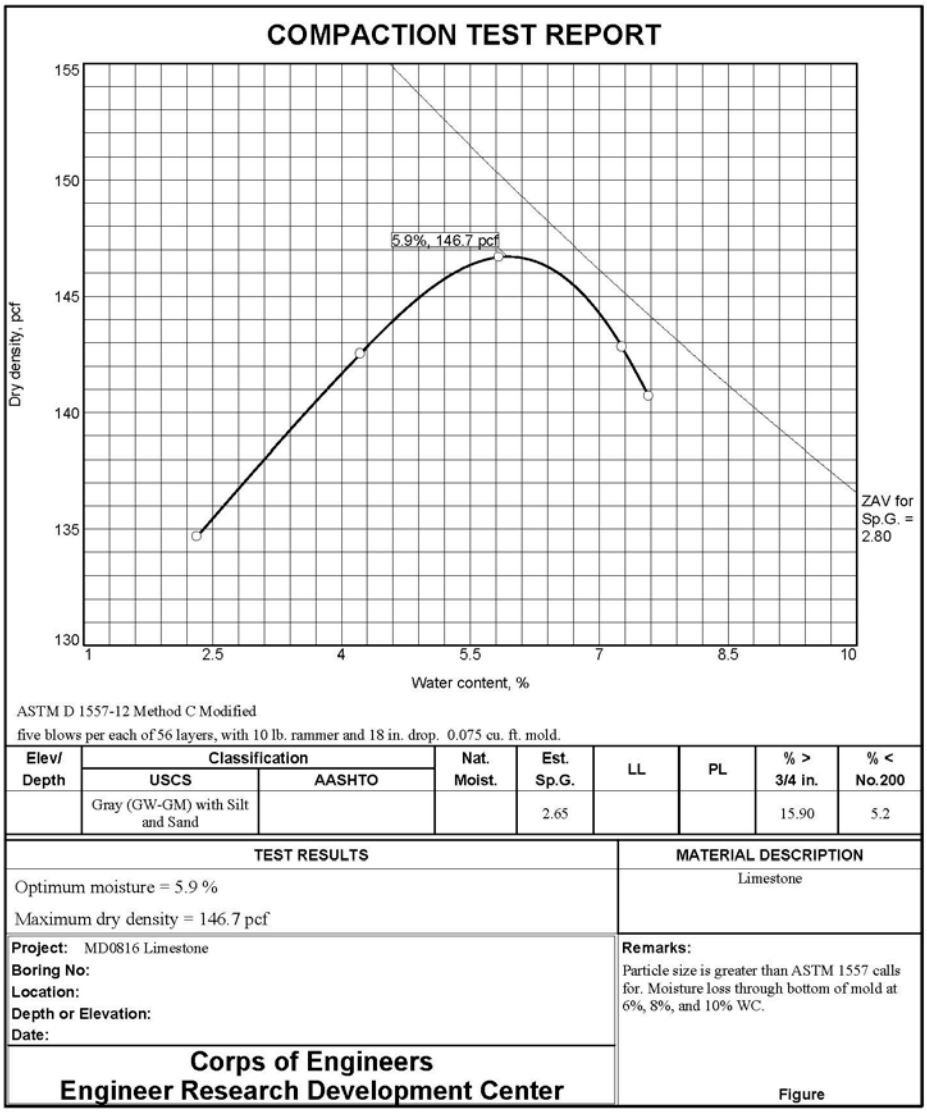

Figure 8. Base Course Moisture-Density Relationship

3.4 HOT-MIX ASPHALT.

The asphalt layer for each test item was constructed using a locally available 12.5-mm nominal maximum aggregate size (NMAS) HMA mixture. Mixture properties were adjusted to closely replicate those used in the Phase I report, "Cyclic Plate Testing of Geogrid-Reinforced Airport Pavements—Phase I" [7]. Pertinent mixture properties, including Phase I values, are presented in table 2.

Table 2. The HMA Mixture Properties

Test Property		Phase I*	Phase II**
N_{design}		85	85
Binder grade		PG 67-22	PG 67-22
Mixing temperature (°F)		320	320
Compaction temperature (°F)		300	300
Percent Passing (%)	1.0 in. (25.0 mm)	100	100
	3/4 in. (19.0 mm)	100	100
	1/2 in. (12.5 mm)	97	95
	3/8 in. (9.5 mm)	86	87
	No. 4 (4.75 mm)	55	57
	No. 8 (2.36 mm)	37	37
	No. 30 (0.60 mm)	20	19
	No. 50 (0.30 mm)	13	12
	No. 200 (0.075 mm)	5.0	5.3
RAP (%)		11	11
RAP AC (%)		5.6	5.6
G_{sb}		2.520	2.520
P_b (%)		5.2	5.4
G_{mm}		2.313	2.366
VMA (%)		13.0	14.1

*Phase I—Cyclic Plate Testing of Geogrid-Reinforced Airport Pavement [7]
**Phase II—Cyclic Plate Testing of Geosynthetic-Reinforced Airfield Pavement
AC = Asphalt content
G_{mm} = Theoretical maximum specific gravity
G_{sb} = Bulk specific gravity
P_b = Percent asphalt binder
N_{design} = Number of gyrations
RAP = Reclaimed asphalt pavement
VMA = Voids in mineral aggregate

3.5 GEOSYNTHETICS.

Four different geosynthetics were evaluated during this study: Tensar BX1200 (BX1200) (figure 9(a)), Tensar TX140 (TX140) (figure 9(b)), HUESKER Fornit 40/40-25T (Fornit 40/40-25T) (figure 9(c)), and TenCate Mirafi RS580*i* (RS580*i*)(figure 9(d)). BX1200 is a biaxial punched and drawn polypropylene geogrid consisting of a series of rectangles. TX140 is a triaxial geogrid consisting of a series of concentric triangles, forming a series of concentric hexagons. Fornit 40/40-25T is comprised of polypropylene yarns manufactured with an interlocking pattern and then coated with a polymer. RS580*i* is a woven geosynthetic manufactured from polypropylene filaments. These products were selected to represent a range of different geosynthetic types.

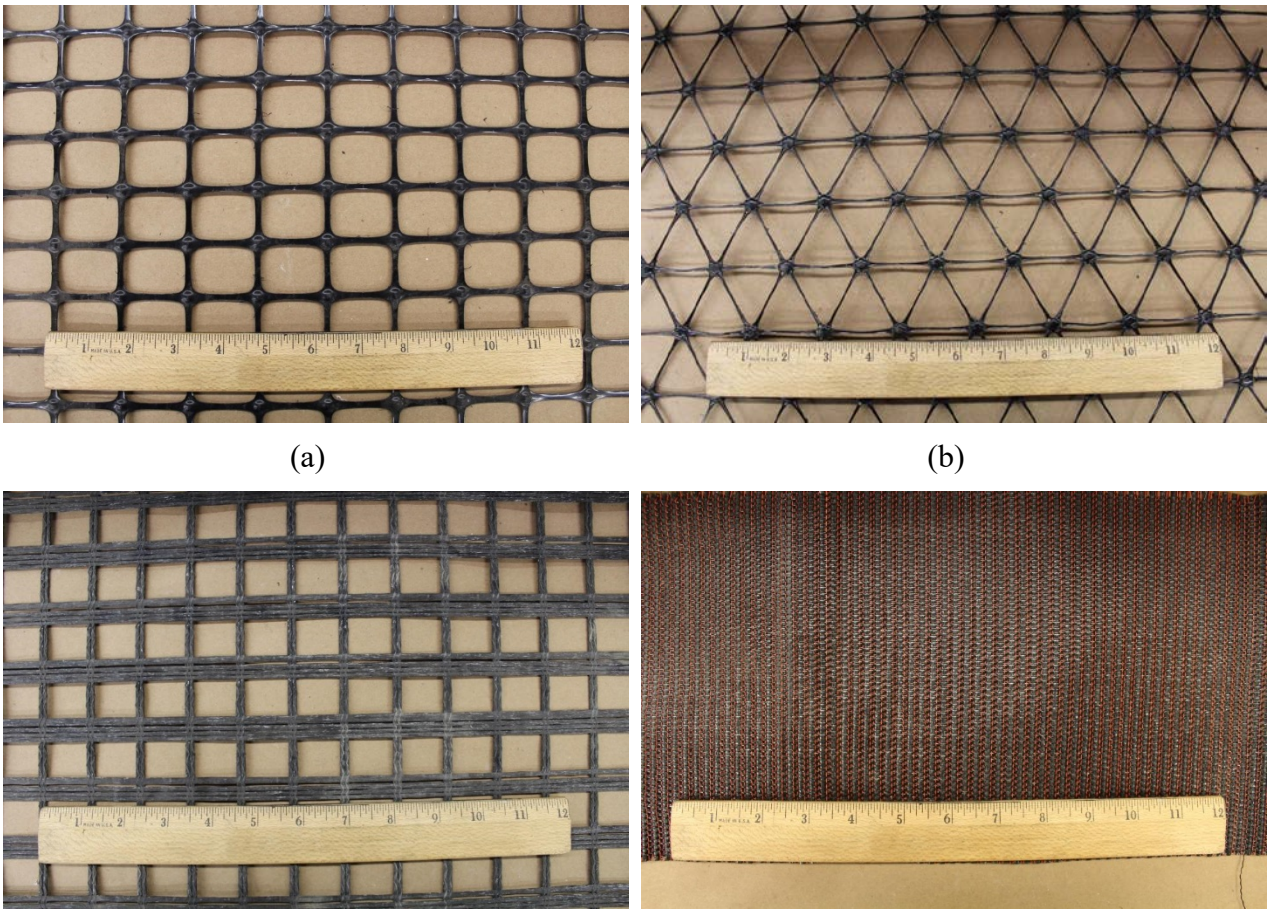

(a) (b)

(c) (d)

Figure 9. Geosynthetics Evaluated: (a) BX1200, (b) TX140, (c) Fornit 40/40-25T, and (d) RS580*i*

4. INSTRUMENTATION.

Sensors were placed in the subgrade, subbase, and at the pavement surface to quantify the response of each test item during loading. The instrumentation profile view is shown in figure 10. These sensors are described in greater detail in the following sections.

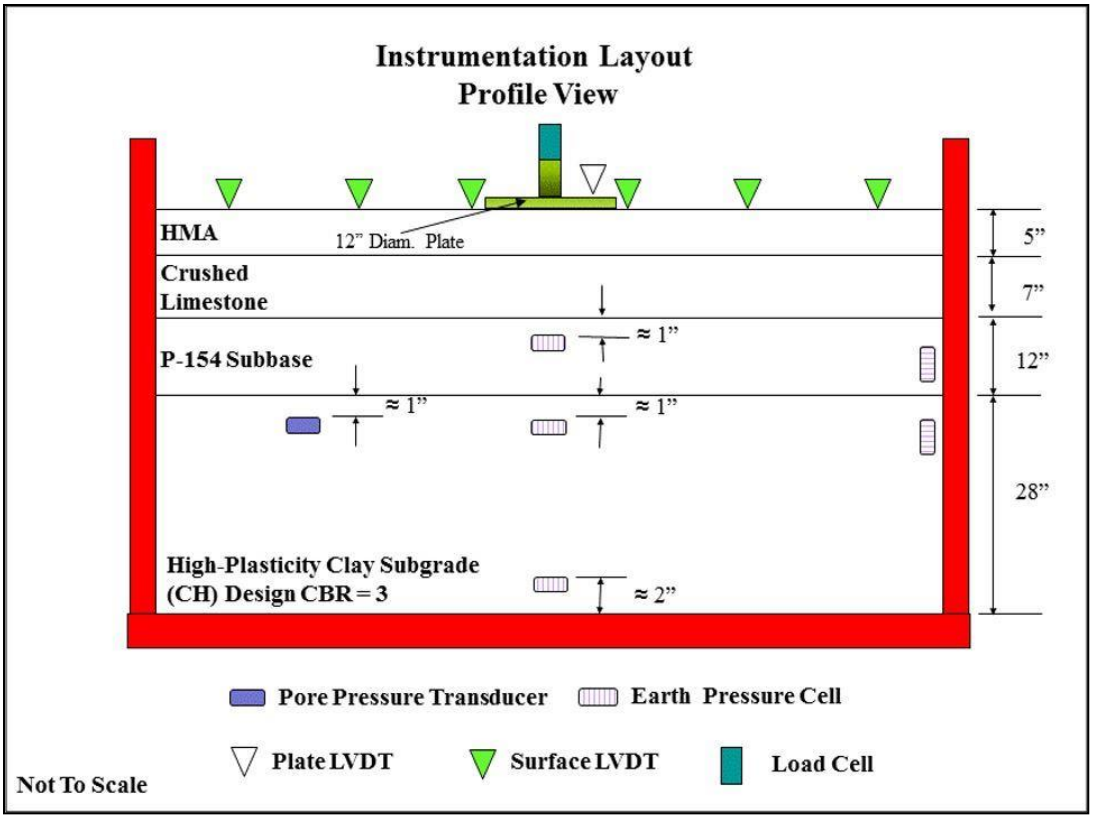

Figure 10. Instrumentation Layout Profile View

4.1 SUBGRADE/SUBBASE INSTRUMENTATION.

Three 4-in.-diameter Geokon® EPCs capable of measuring earth pressures up to 58 psi were placed near the top and bottom of the subgrade as shown in figure 11. The upper EPC was placed approximately 1 in. below the subbase-subgrade interface, and the lower EPC was placed approximately 2 in. above the bottom of the test item. Both EPCs were placed directly under the loading plate center. Lastly, one EPC was placed vertically, approximately 2 in. from the test box wall and approximately 1 in. below the subbase-subgrade interface, to monitor lateral earth pressure and to quantify the effect, if any, of wall constraints on load distribution.

Two 4-in.-diameter Geokon EPCs capable of measuring earth pressures up to 147 psi were placed in the subbase. One EPC was placed directly under the loading plate center, approximately 1 in. below the subbase surface. One EPC was placed vertically approximately 2 in. from the test box wall and approximately 1 in. below the base-subbase interface.

Figure 11. Subgrade EPC Installation

4.2 SURFACE INSTRUMENTATION.

A series of seven LVDTs were placed at the HMA layer surface to measure vertical displacement on the test item surface. The sensor offsets relative to the loading plate center are shown in figure 12.

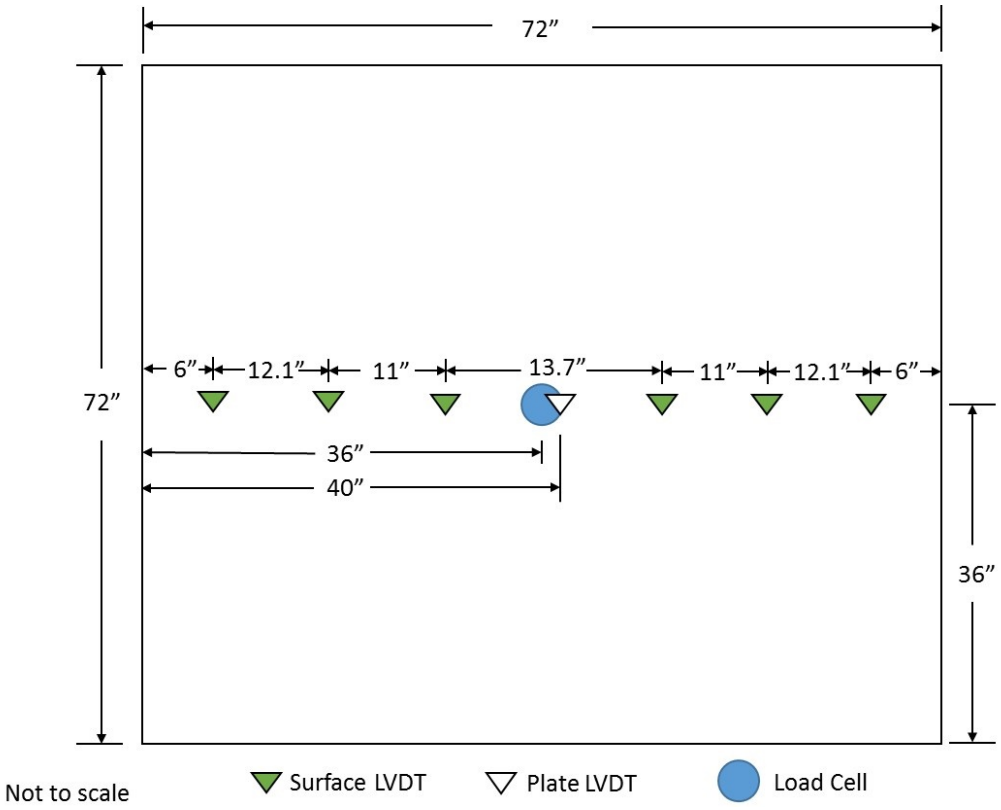

Figure 12. Surface Instrumentation Plan View

5. AS-BUILT PAVEMENT PROPERTIES AND CHARACTERIZATION.

Quality control tests were performed during construction of each material lift to ensure target values were achieved and to monitor material consistency. Dry density and moisture content were measured using a nuclear moisture density device in accordance with ASTM D6938-17a [8] to verify the uniformity of each material lift. Field in-place CBR tests were performed in general accordance with ASTM D4429-09a [9] on each compacted lift. To further characterize the strength of the completed base and subgrade layers, dynamic cone penetrometer (DCP) tests were performed in accordance with ASTM D6951-09 [10]. Asphalt cores were obtained from each test item, and core densities were determined in accordance with AASHTO T 166 [11]. Material test properties, including standard deviation, are summarized in table 3.

Table 3. As-Built Material Properties Summary

Property	Control (FAAP-154)	Control (ERDC P-154) (3 CBR)	Control (ERDC P-154) (2 CBR)	BX1200	TX140	Fornit 40/40-25T	RS580*i*
Test Item	1	6	7	2	3	4	5
CH Subgrade Properties							
Wet density (pcf)	113.4 ±1.5	111.2 ±1.2	107.6 ±1.4	112.0 ±1.1	111.5 ±2.7	110.4 ±1.7	111.5 ±1.3
Dry density (pcf)	84.4 ±1.6	81.8 ±1.3	78.6 ±2.3	82.3 ±1.4	79.9 ±3.7	81.3 ±1.4	81.5 ±1.5
Nuclear moisture (%)	34.4 ±1.5	36.0 ±1.2	38.1 ±2.8	36.2 ±1.4	39.6 ±3.3	36.1 ±1.3	36.8 ±1.6
Oven-dried moisture (%)	36.8 ±0.9	38.2 ±0.9	40.7 ±2.6	38.6 ±1.1	38.0 ±1.5	39.2 ±2.0	38.0 ±1.9
In-place CBR (%)	3.0 ±0.2	2.9 ±0.3	1.8 ±0.1	2.9 ±0.2	3.0 ±0.4	2.9 ±0.2	2.8 ±0.2
Thickness (in.)	27.9 ±0.1	27.8 ±0.1	28.0 ±0.1	28.0 ±0.2	27.9 ±0.1	28.1 ±0.1	28.1 ±0.1
P-154 Subbase Properties							
Wet density (pcf)	140.3 ±1.1	110.5 ±0.5	114.8 ±1.0	110.0 ±1.5	113.9 ±0.7	110.6 ±1.5	111.8 ±0.5
Dry density (pcf)	131.6 ±0.9	106.1 ±0.1	110.3 ±1.1	106.0 ±1.6	110.8 ±0.9	108.1 ±1.5	108.2 ±0.3
Nuclear moisture (%)	6.6 ±0.3	4.1 ±0.4	4.0 ±0.4	3.8 ±0.4	2.8 ±0.3	2.4 ±0.2	3.3 ±0.2
Oven-dried moisture (%)	3.1 ±0.2	4.3 ±0.1	5.0 ±0.1	4.1 ±05	2.3 ±0.2	3.5 ±0.2	3.2 ±0.1
In-place CBR (%)	55 ±5	18	18	16	18	17	17
Thickness (in.)	11.9 ±0.3	12.1 ±0.1	12.0 ±0.1	12.0 ±0.2	12.0 ±0.1	11.9 ±0.1	12.1 ±0.1
Crushed Limestone Base Properties							
Wet density (pcf)	141.1 ±2.7	137.9 ±2.6	138.4 ±1.7	140.9 ±1.4	139.1 ±1.4	138.2 ±1.9	139.1 ±0.9
Dry density (pcf)	137.4 ±2.7	134.2 ±2.4	135.7 ±1.7	135.0 ±1.3	135.6 ±1.2	135.3 ±2.2	136.4 ±0.8
Nuclear moisture (%)	2.8 ±0.1	2.8 ±0.2	2.0 ±0.2	4.4 ±0.1	2.6 ±0.1	2.2 ±0.3	2.0 ±0.1
Oven-dried moisture (%)	1.9 ±0.2	2.5 ±0.2	1.3 ±0.2	2.1 ±0.1	2.0 ±0.2	0.9 ±0.2	1.3 ±0.1
In-place CBR (%)	100+	100+	100+	100+	100+	100+	100+
Thickness (in.)	7.2 ±0.3	6.8 ±0.1	6.8 ±0.1	6.9 ±0.1	6.9 ±0.1	7.0 ±0.1	6.9 ±0.1

Table 3. As-Built Material Properties Summary (Continued)

Property	Control (FAAP-154)	Control (ERDC P-154) (3 CBR)	Control (ERDC P-154) (2 CBR)	BX1200	TX140	Fornit 40/40-25T	RS580*i*
Item	1	6	7	2	3	4	5
HMA Properties							
Density (% of G_{mm})	94.5*	94.5*	94.5*	94.5*	94.5*	94.5*	94.5*
Thickness (in.)	4.7±0.1	5.3±0.1	4.9±0.2	5.2±0.1	4.9±0.1	5.2±0.1	4.9±0.1

*Asphalt density based on average of two asphalt cores taken randomly prior to saw-cutting slabs.

6. RESULTS.

The number of cycles to achieve 1 in. and 2 in. of permanent deformation are presented in table 4. Additionally, the TBRs, which are defined by AASHTO R 50-09 [1] as the ratio of the number of load cycles of a reinforced pavement structure to reach a defined failure state to the number of load cycles of an identical unreinforced pavement structure, were calculated at 1 in. and 2 in. of permanent surface deformation. In terms of cycles-to-failure at the 2-in. failure criteria, BX1200 was found to be the best performer having a TBR of 2.6, followed by RS580*i*. It is noted that RS580*i* had a TBR less than 1.0 at 1 in. of permanent deformation, suggesting that some level of deformation is required to mobilize a performance benefit. Fornit 40/40-25T was found to perform slightly better than the control having a TBR of 1.1 at 1 in. and 1.0 at 2 in. deformation. TX140 was found to have a TBR of 0.6 when compared to the control (3 CBR). A review of the construction data indicates that the TX140 item had lower subgrade density and higher subgrade density variability than the other items. Additionally, it is observed that the TX140 item was found to have approximately 0.5 in. less asphalt than the unreinforced item. The combination of these two material properties could explain the reduced performance in the TX140 item when compared to the unreinforced section. The unreinforced section containing the FAA-provided P-154 was the overall best performer in the test sequence, which was expected as a result of the much higher subbase strength characteristics. The 2 CBR item performed approximately 20% worse than the 3 CBR item, which was expected because of the reduced subgrade strength.

Table 4. Cycles-to-Failure and TBR

Item	Cycles at 1-in. Permanent Deformation	Cycles at 2-in. Permanent Deformation	TBR at 1-in. Permanent Deformation	TBR at 2-in. Permanent Deformation
Control (FAA P-154)	150,720	N/A*	-	-
Control (ERDC P-154) (3 CBR)	3,700	16,990	1	1
Control (ERDC P-154) (2 CBR)	3,000	14,000	0.8*	0.8*
BX1200	9,720	44,960	2.6	2.6
TX140	1,460	9,890	0.4	0.6
Fornit 40/40-25T	4,100	17,600	1.1	1.0
RS580*i*	2,575	20,830	0.7	1.2

*Ratio of cycles-to-failure for 2 CBR to 3 CBR Control for information only
**This is not applicable because the test was terminated due to unreasonably high cycles.

Permanent deformation data measured directly at the load plate are shown in figure 13. In the suite of items containing ERDC P-154, the test item that incorporated BX1200 was found to be the best performer at all load cycles, while the TX140 item was found to be the worst performer. Fornit 40/40-25T was found to have approximately equivalent performance to the unreinforced control item at all load levels. RS580*i* was found to underperform the unreinforced item up to approximately 10,000 cycles (1.5 in. of permanent deformation), after which some performance improvement was observed, suggesting that some level of permanent deformation is required to engage the geotextile-reinforcing benefit.

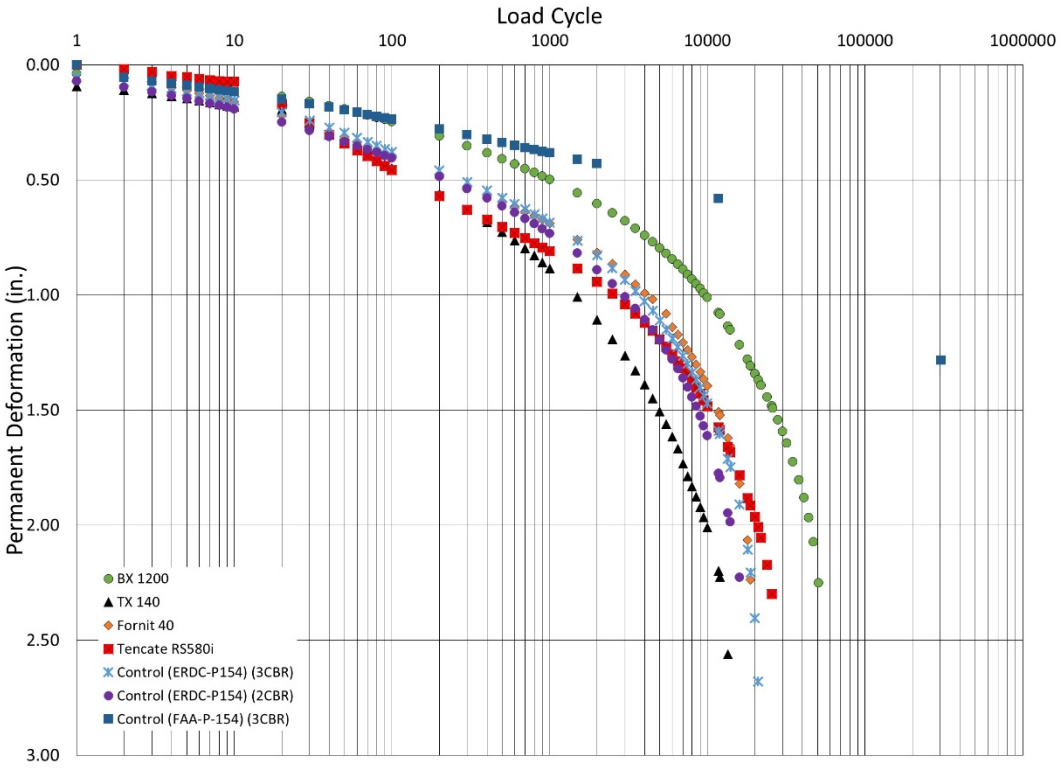

Figure 13. Permanent Surface Deformation Measured at the Load Plate

Dynamic deformation data (the difference in peak deformation and permanent deformation) were calculated for each test item and are presented in figure 14. Dynamic deformation was generally consistent for each item until approaching failure at which the dynamic deformation was observed to increase. A review of the data indicated that dynamic deformations were relatively small in magnitude, ranging from approximately 0.06 to 0.10 in. Elastic strain does not appear to be a good indicator of performance for geosynthetic-reinforced pavement structures.

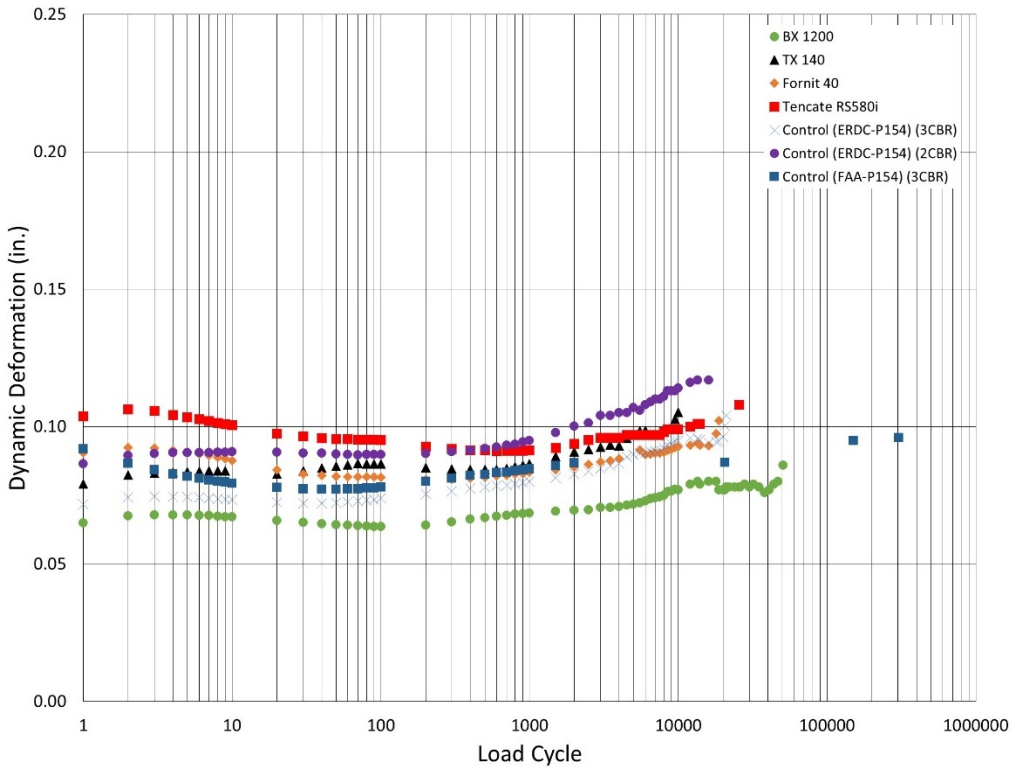

Figure 14. Dynamic Vertical Deformation Measured at the Load Plate

EPC response data were collected to characterize material response with load cycles. Measured maximum vertical pressure at the top of subbase is shown in figure 15. It was observed that subbase pressures were found to slightly increase and then decrease after initial loading, likely attributed to aggregate shakedown. After a duration of constant or decreased pressure with loading, it was found that the measured vertical pressure increased. A review of the data indicated that maximum pressure inflection points were observed around 1 in. of permanent deformation. The general shape of subbase pressure curves was consistent for all items. It is noted that for the FAA P-154 test item, subbase pressure was found to be relatively consistent for the duration of loading, after initial aggregate shakedown.

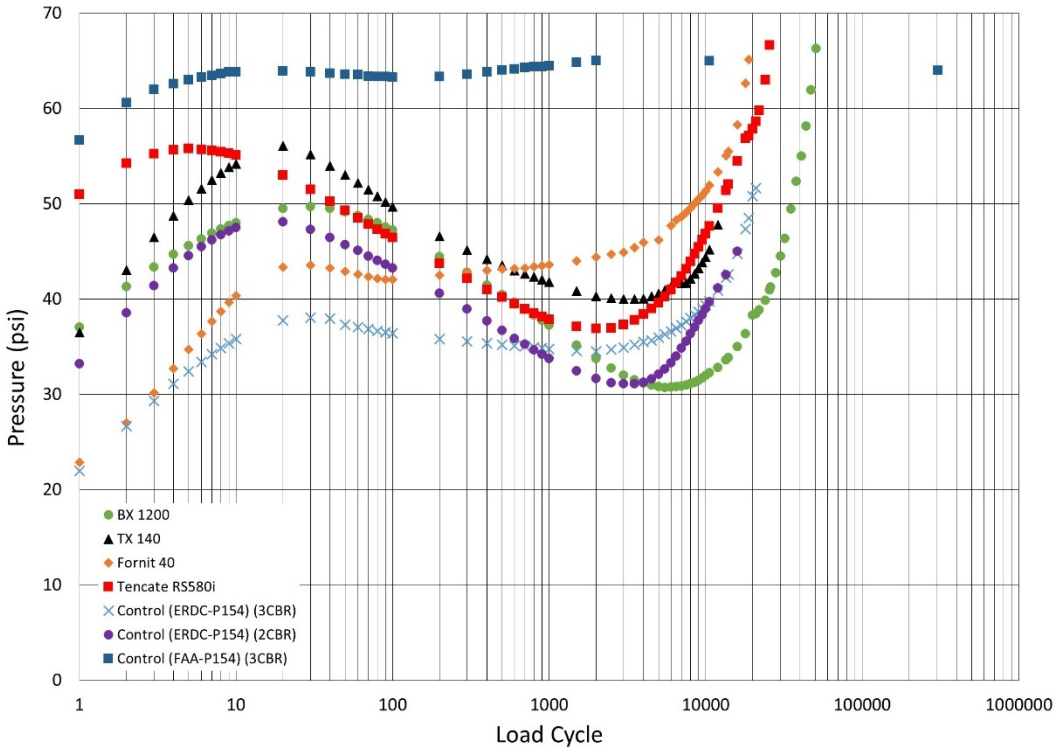

Figure 15. Maximum Vertical Pressure Response Data at Top of Subbase

Measured maximum vertical pressure at the top of subgrade is shown in figure 16 and was found to be relatively constant up to 1000 cycles for all items. Thereafter, the vertical pressure increased, which could be attributed to an increase in subgrade rutting. The subgrade maximum pressure curves general shape was generally consistent for all items. Pressure response for the FAA P-154 test item was relatively consistent throughout test duration.

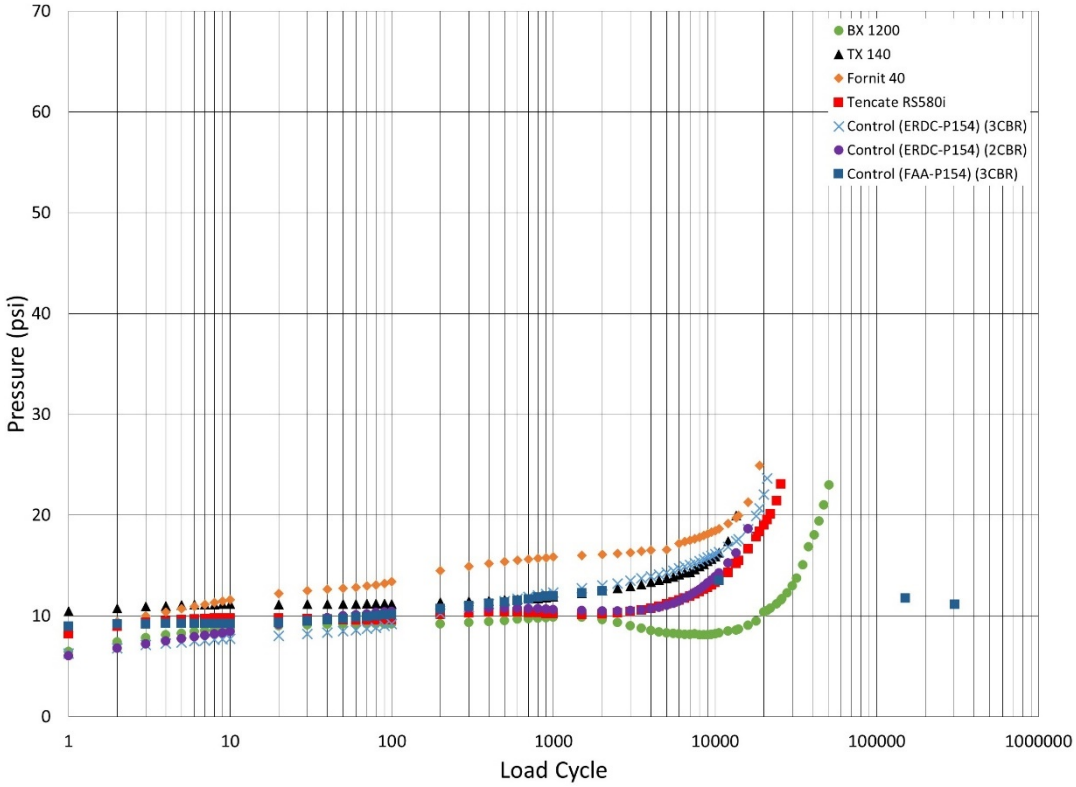

Figure 16. Maximum Vertical Pressure Response Data at Top of Subgrade

Vertical pressure response data at the bottom of subgrade is presented in figure 17. A response data review indicated that two distinct behavior shapes were identified. It was observed that the BX1200 and RS580*i* test items displayed similar response behavior over loading duration, and the BX1200 test item had lower measured pressures than the RS580*i*, which was consistent with permanent deformation observations. Additionally, pressures for these two test items were found to display a relatively constant increase with an increase in surface deformation.

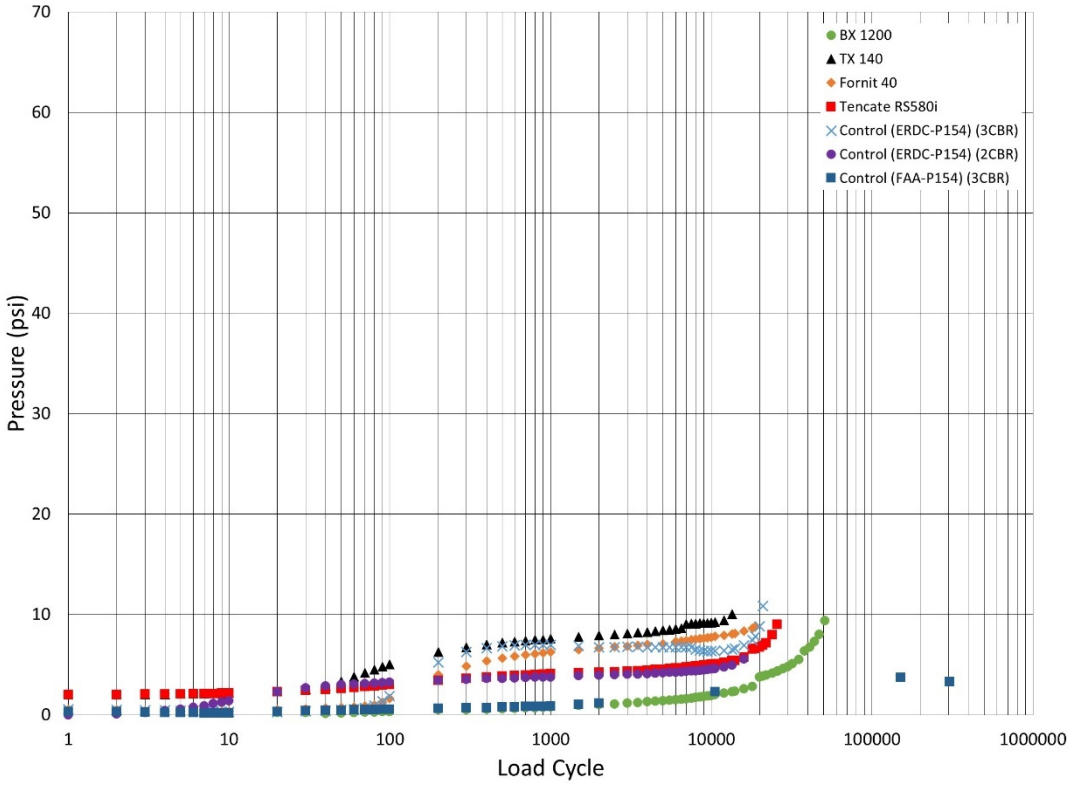

Figure 17. Vertical Pressure Response Data at Bottom of Subgrade

The TX140, Fornit 40/40-25T, and Control (ERDC P-154 3 CBR and 2 CBR) test items displayed similar behaviors that were found to be different from the two best performers. It was observed that a significant increase in bottom of subgrade pressure occurred early in loading (around 20 to 60 cycles) which was found to be at approximately 0.25 in. of permanent deformation. Pressure was observed to remain constant or slightly increase after this point.

At the conclusion of testing, a forensic investigation was performed to observe deformation in each layer and to quantify changes in material properties. Data collected included elevation and rut depth measurements at the asphalt surface and elevation, rut depth, CBR, and density data of the base, subbase, and subgrade layers. A summary of individual layer deformation, which is the difference in surface elevation from pre-test and post-test elevation measurements, is presented in table 5. Permanent layer deformation plots for each test item are presented in figures 18 through 24.

Table 5. Post-Test Layer Deformation

Test Item	Individual Layer Permanent Deformation (in.)			
	Asphalt	Base	Subbase	Subgrade
Control (FAA P-154)	1.2	0.5	0.5	0.2
Control (ERDC P-154) (3 CBR)	2.5	2.6	2.5	0.8
Control (ERDC P-154) (2 CBR)	2.3	2.0	2.2	0.5
BX1200	2.2	2.2	2.3	0.6
TX140	2.6	2.5	2.4	1.3
Fornit 40/40-25T	2.2	2.0	2.0	0.7
RS580*i*	2.3	2.2	2.3	0.4

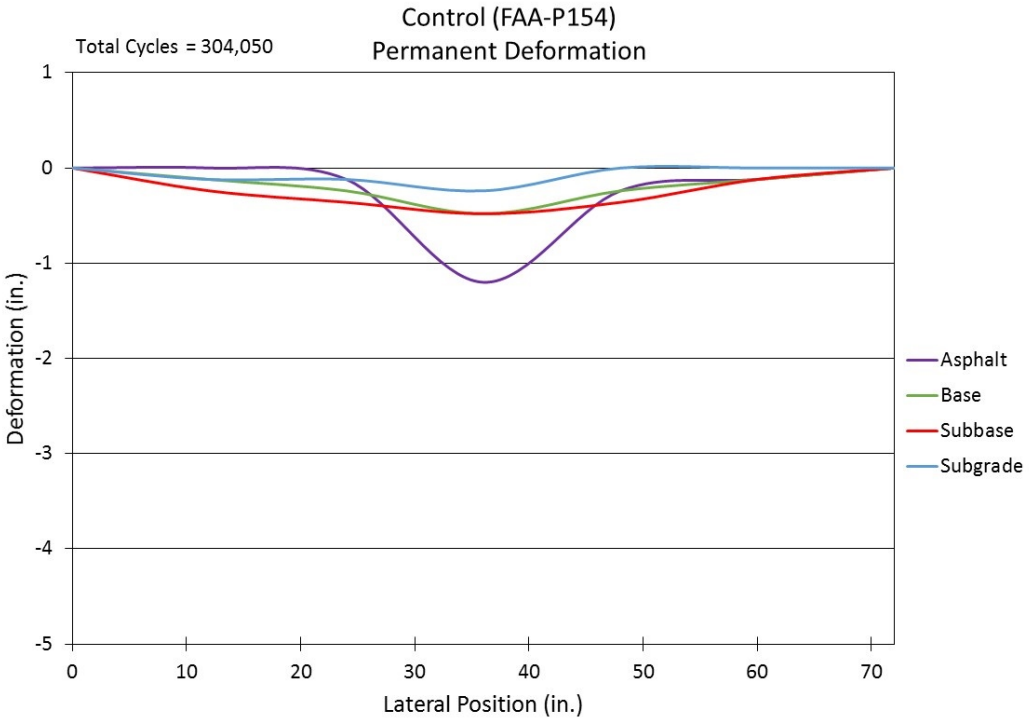

Figure 18. Permanent Layer Deformation for FAA P-154 Unreinforced Item

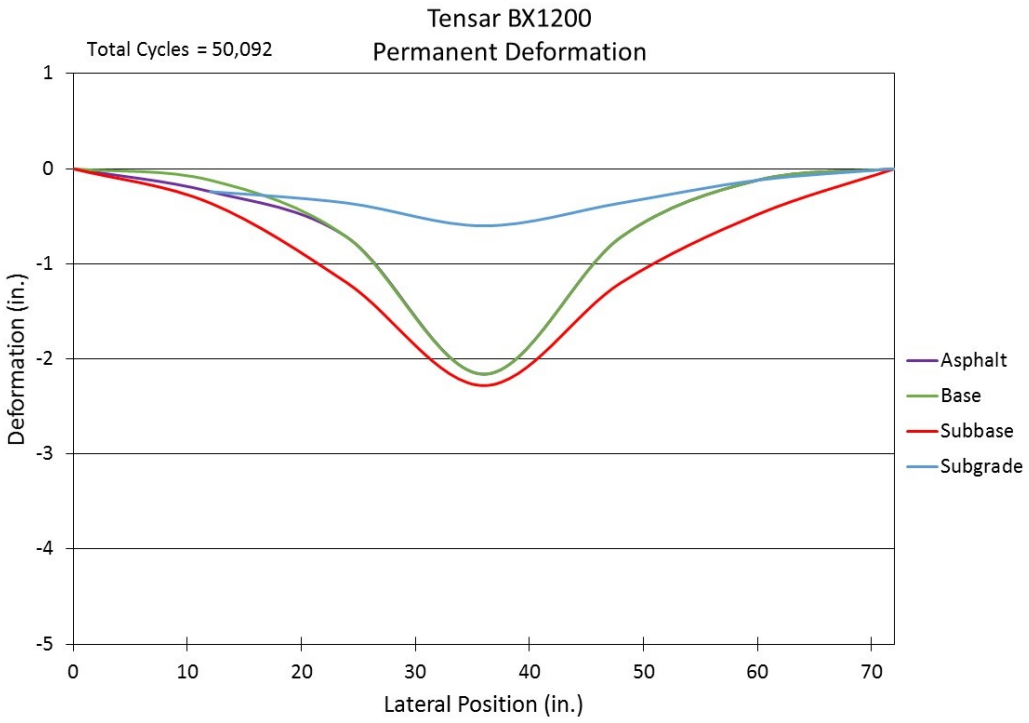

Figure 19. Permanent Layer Deformation for BX1200 Reinforced Item

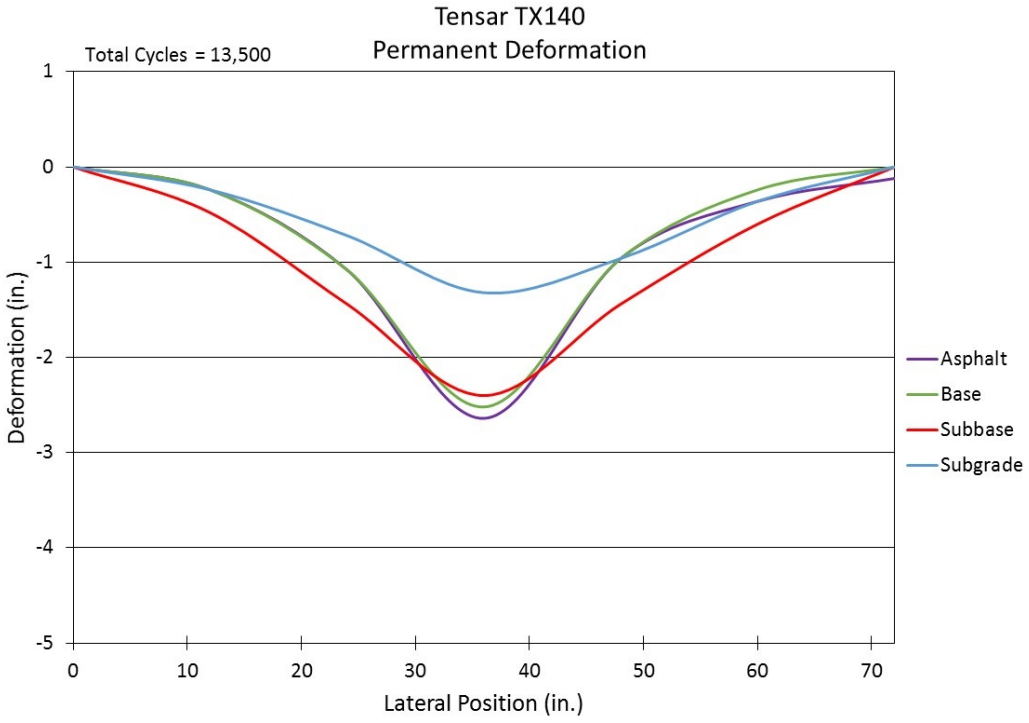

Figure 20. Permanent Layer Deformation for TX140 Reinforced Item

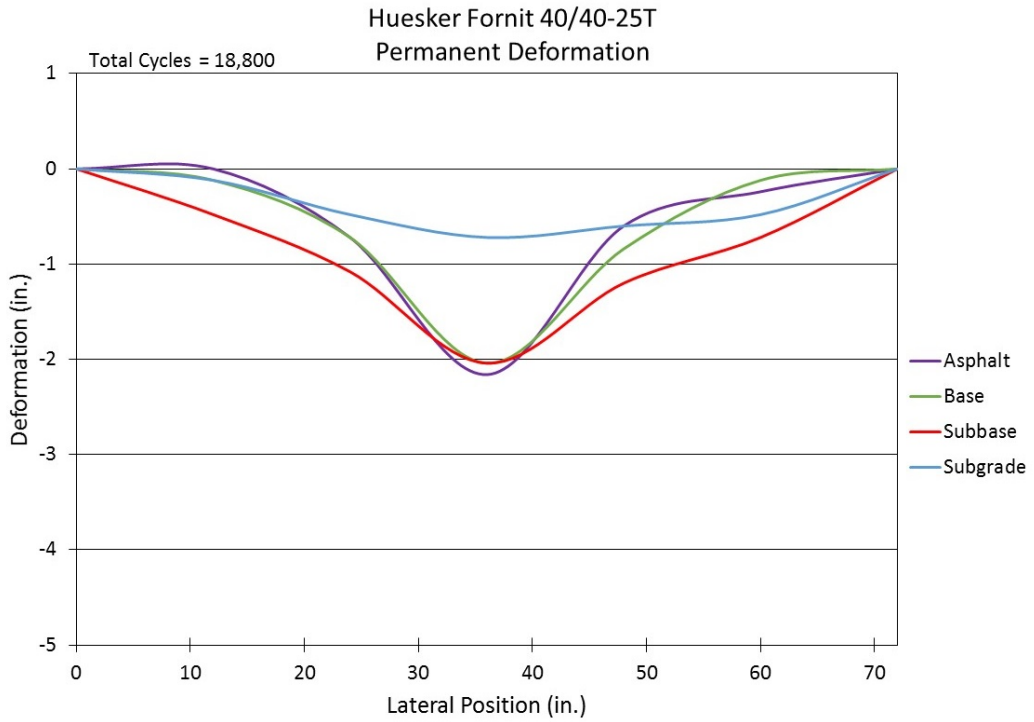

Figure 21. Permanent Layer Deformation for Fornit 40/40-25T Reinforced Item

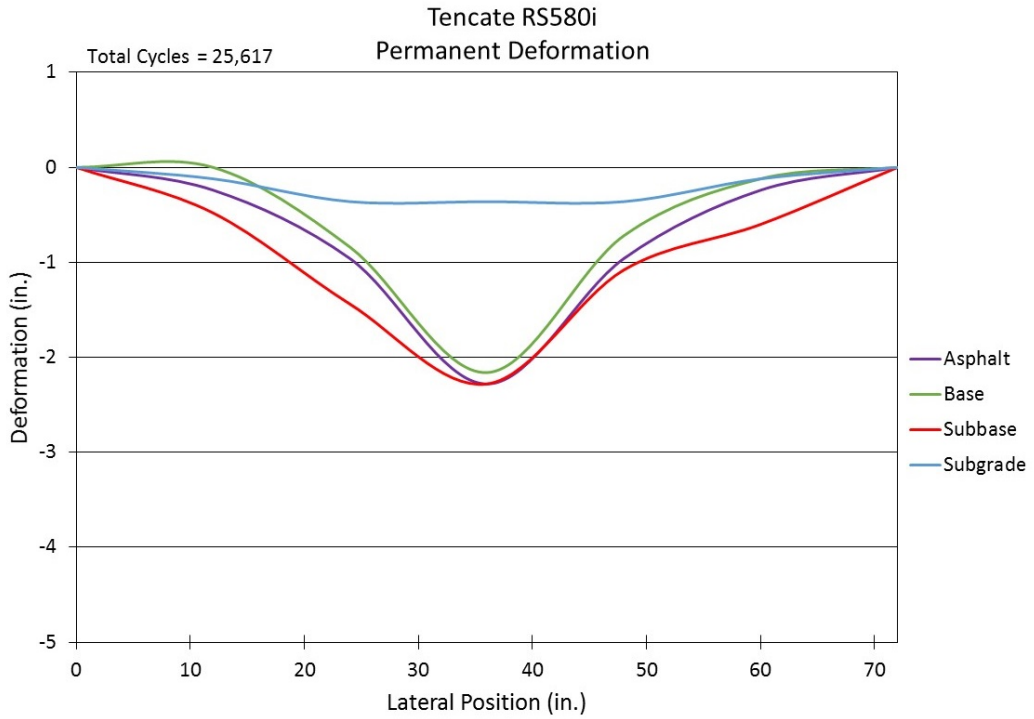

Figure 22. Permanent Layer Deformation for RS580*i* Reinforced Item

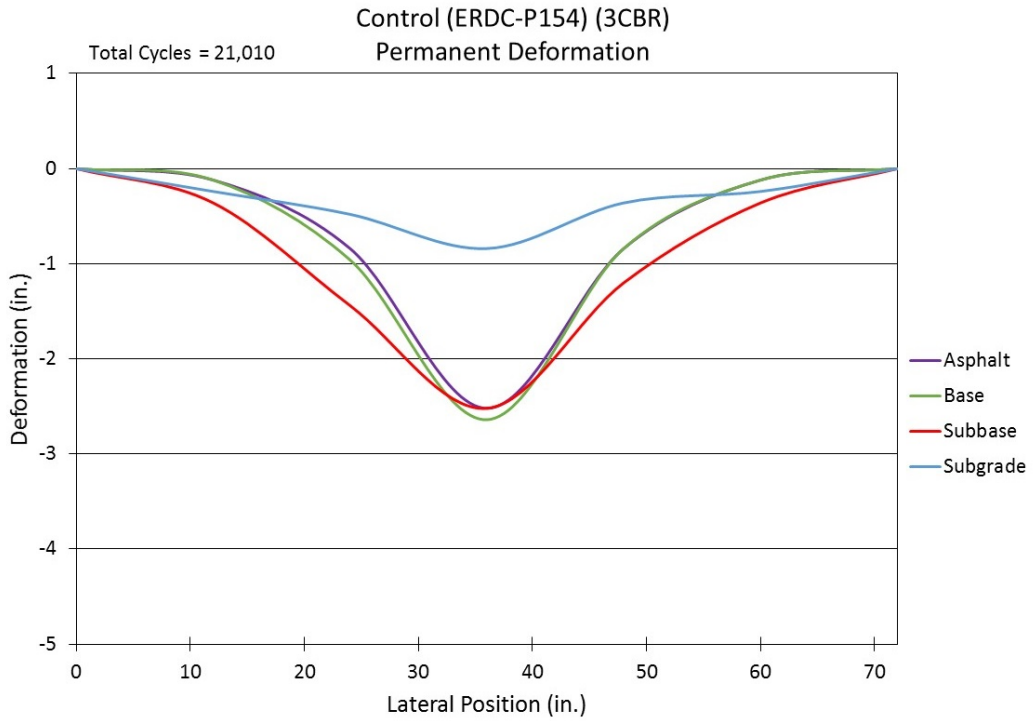

Figure 23. Permanent Layer Deformation for ERDC P-154 (3 CBR) Unreinforced Item

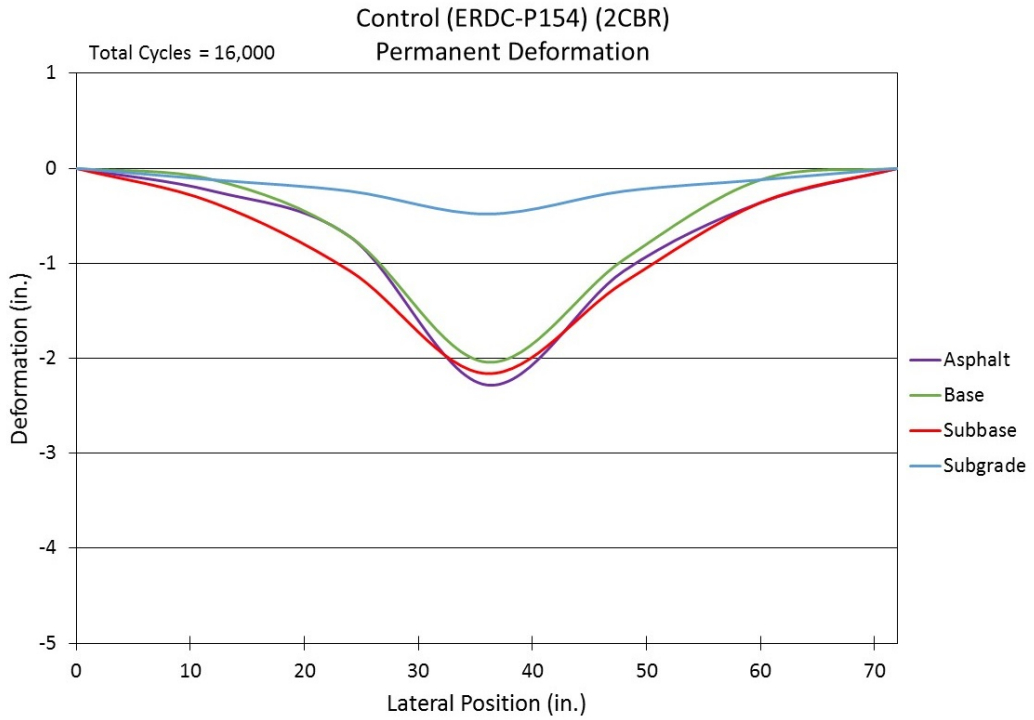

Figure 24. Permanent Layer Deformation for ERDC P-154 (2 CBR) Unreinforced Item

Post-test material properties are presented in table 6. Nuclear density values were obtained outside the primary observed deflection basin in each layer. In general, minor changes in dry density and moisture content were observed in each component layer.

In terms of CBR, more significant changes were observed. For the CH layer, generally higher CBR values were observed post-traffic, particularly in test items that sustained more load cycles, which could be attributed to layer densification. CBR values in the subbase layer were found to be consistent with pre-test values, with the exception of the FAA P-154 unreinforced test item, which displayed a significant increase in CBR that could be attributed to both the significant level of load cycles and potential natural aggregate cementation. Test results showed that the crushed stone base layer decreased in CBR ranging from approximately 20% to 60%, which could be attributed to particle reorientation from the approximately 2-in. permanent deformation observed. Additionally, although care was taken during excavation, some minimal surface disturbance could influence CBR determination.

Photographs of each excavated cross-section are shown in figure 25. Orange markers were used to delineate each layer interface and to highlight deformation observed in each layer.

Table 6. Post-Test Material Properties Summary

Property	Control (FAA P-154)	Control (ERDC P-154) (3 CBR)	Control (ERDC P-154) (2 CBR)	BX1200	TX140	Fornit 40/40-25T	RS580*i*
CH Subgrade Properties							
Wet density (pcf)	113.4 ±0.8	111.3 ±0.7	111.2 ±2.1	111.2 ±0.6	109.6 ±1.2	109.5 ±0.6	109.9 ±1.3
Dry density (pcf)	83.9 ±0.8	82.3 ±0.8	77.6 ±2.4	80.3 ±1.4	79.7 ±1.4	78.1 ±0.5	79.7 ±0.9
Nuclear moisture (%)	35.2 ±1.5	35.3 ±1.1	43.5 ±1.9	38.5 ±2.3	37.6 ±0.9	40.3 ±1.5	37.8 ±1.0
Oven-dried moisture (%)	36.1 ±2.0	38.2 ±1.3	41.1 ±0.4	36.2 ±1.0	38.7 ±1.3	38.3 ±0.7	38.6 ±1.5
In-place CBR (%)	5.1 ±0.8	3.3 ±0.5	1.9 ±0.2	4.3 ±0.4	2.7 ±0.6	3.3 ±0.5	3.0 ±0.4
P-154 Subbase Properties							
Wet density (pcf)	132.6 ±0.9	114.2 ±0.5	114.5 ±0.9	113.8 ±07	113.7 ±2.0	112.1 ±0.5	112.3 ±0.9
Dry density (pcf)	127.1 ±1.0	111.1 ±0.6	110.6 ±0.8	111.2 ±0.6	111.1 ±2.1	109.6 ±0.6	109.8 ±0.8
Nuclear moisture (%)	4.3 ±0.5	2.7 ±0.2	3.5 ±0.1	2.4 ±0.2	2.4 ±0.2	2.2 ±0.1	2.3 ±0.2
Oven-dried moisture (%)	3.7 ±0.1	2.4 ±0.2	3.4 ±0.2	2.2 ±0.2	2.0 ±0.2	2.2 ±0.5	1.4 ±0.3
In-place CBR (%)	100+	16	18	20	19	17	17
Crushed Limestone Base Properties							
Wet density (pcf)	141.7 ±2.9	134.7 ±1.6	135.6 ±3.1	136.7 ±2.1	138.6 ±1.2	133.7 ±1.0	139.7 ±1.1
Dry density (pcf)	137.6 ±3.2	131.1 ±1.4	132.3 ±3.5	133.7 ±0.3	135.2 ±0.2	130.9 ±0.2	136.9 ±0.4
Nuclear moisture (%)	3.0 ±0.5	2.7 ±0.2	2.5 ±0.4	2.1 ±0.3	2.5 ±0.2	2.1 ±0.2	2.0 ±0.4
Oven-dried moisture (%)	2.3 ±0.1	2.5 ±0.2	1.7 ±0.2	1.9 ±0.2	2.5 ±0.2	1.5 ±0.2	1.7 ±0.2
Inside rut CBR (%)	100+	69	44	74	64	42	86
Outside rut CBR (%)	NA	62	75	100	100	34	79

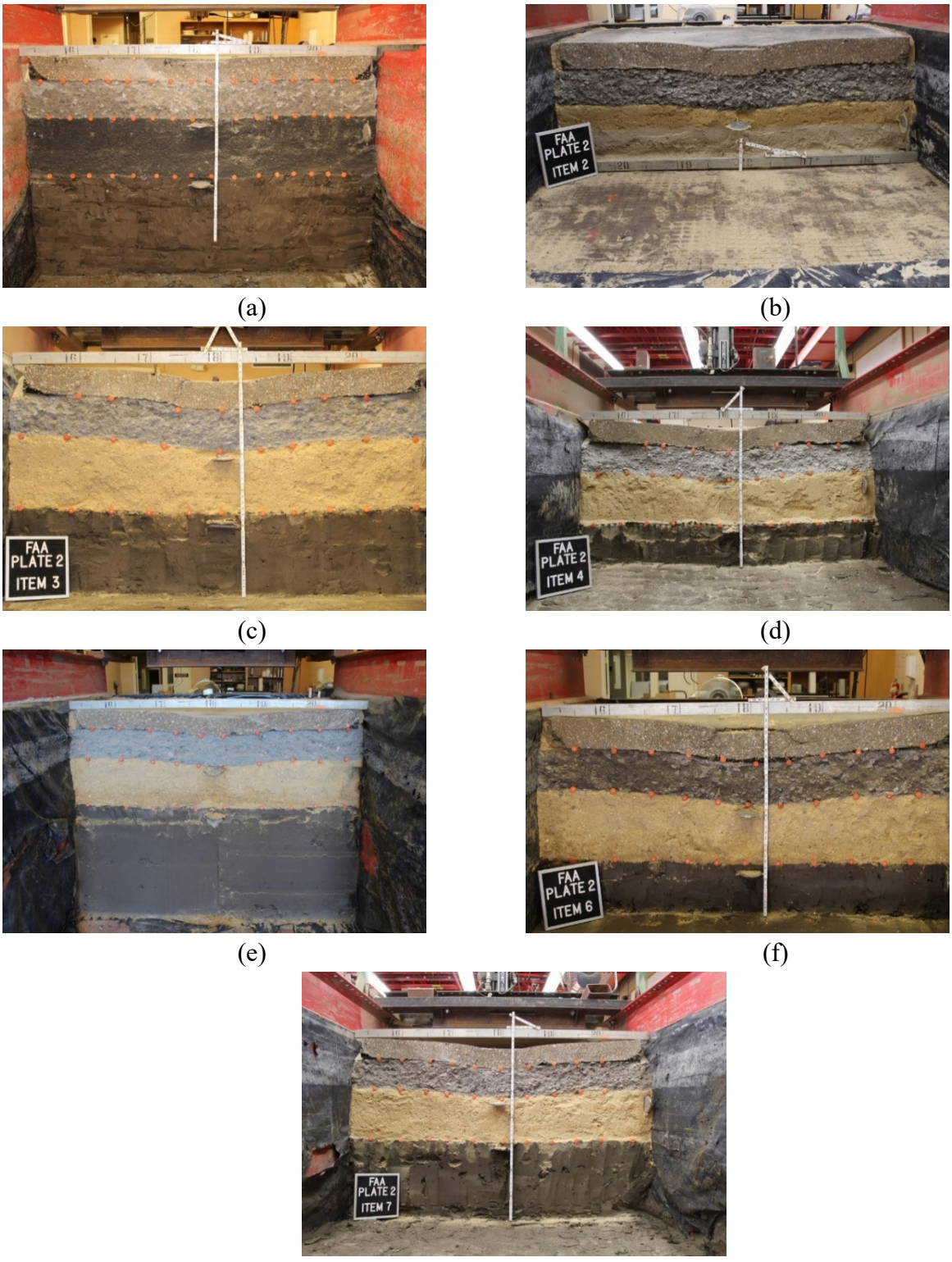

(a) (b) (c) (d) (e) (f) (g)

Figure 25. Post-Test Excavated Cross-Section for (a) Control FAA P-154, (b) BX1200, (c) TX140, (d) Fornit 40/40-25T, (e) RS580*i*, (f) Control ERDC P-154 (3 CBR), and (g) Control ERDC P-154 (2 CBR) Test Items

7. COMPARSION OF PHASE I AND PHASE II PLATE LOADING DATA.

Phase I of this study included cyclic plate load testing of a series of test items with the same pavement structure, same loading conditions, and similar geosynthetics [7], although the geosynthetics were placed at the base-subbase interface. The companion study's intent was to compare the effect of geosynthetic placement location on measured pavement performance. A summary of the Phase I test items is provided in table 7. It is noted that Phase I incorporated HUESKER Fornit 30/30, while Phase II incorporated HUESKER Fornit 40/40-25T. A summary of properties for these geosynthetic products is provided in table 8.

Table 7. Phase I Cyclic Plate Test Properties

Property	Control	BX1200	TX140	Fornit 30/30
CH Subgrade Properties				
Wet density (pcf)	110.3	113.5	112.9	114.3
Dry density (pcf)	83.1	85.8	84.7	86.2
Nuclear moisture content (%)	32.7	32.6	33.4	32.5
Oven-dried moisture (%)	35.4	36.9	38.3	36.8
In-place CBR (%)	3.6	3.2	3.4	3.1
Thickness (in.)	27.8	28.4	28.9	28
P-154 Subbase Properties				
Wet density (pcf)	115.5	112.9	113.4	113.6
Dry density (pcf)	110.1	109.4	108.5	109.7
Nuclear moisture content (%)	4.9	3.2	4.5	3.6
Oven-dried moisture (%)	5.8	5.9	5.8	4.2
In-place CBR (%)	15	18	15	15
Thickness (in.)	12.2	12.3	12.4	12.4
Crushed Limestone Base Properties				
Wet density (pcf)	141.4	139.2	140.2	140.2
Dry density (pcf)	134.3	136.4	137.9	137.9
Nuclear moisture content (%)	5.3	2.1	1.7	1.7
Oven-dried moisture (%)	5.1	5.1	4.8	4.8
In-place CBR (%)	88	100+	100+	100+
Thickness (in)	7.1	6.7	6.0	6.7
HMA Properties				
Density (% of G_{mm})	91.2	91.2	91.2	91.2
Thickness (in.)	4.8	5.1	5.0	5.1
Cycles-to-Failure				
Cycles at 1-in. deformation	304	6,322	1,000	9,024
Cycles at 2-in. deformation	1,278	25,960	4.304	34,901

Table 8. HUESKER Fornit Geosynthetic Properties

Property	Fornit 40/40-25T	Fornit 30/30	Difference
Aperture shape	Square	Square	--
Aperture size MD (mm)	25	15	10
Aperture size CMD (mm)	25	15	10
Tensile strength @ 2% Strain MD (kN/m)	15	8	7
Tensile strength @ 2% Strain CMD (kN/m)	15	13	2
Tensile strength @ 5% Strain MD (kN/m)	32	20	12
Tensile strength @ 5% Strain CMD (kN/m)	32	27	5
Ultimate tensile strength MD (kN/m)	40	27	13
Ultimate tensile strength CMD (kN/m)	40	35	5

kN/m = Kilo-Newton meter
MD = Machine direction
CMD = Cross-machine direction

Cycles-to-failure for control items from Phases I and II were found to be significantly different, making it difficult to compare performance with regard to geosynthetic placement location. Data were tabulated to observe material properties that could have contributed to performance differences and are presented in table 9. It was found that, in terms of dry density, Phase I control properties were generally higher or equal to Phase II control properties for the subgrade, subbase, and base courses, suggesting that performance should have been slightly better in Phase I. However, a review of asphalt density data indicated that asphalt density and asphalt thickness was 3% and 0.5 in. lower in Phase I than in Phase II, respectively. These differences in asphalt properties could explain the significantly different performance between the two phases.

The TBRs for each phase are presented in table 10 and are calculated based on the respective unreinforced item in each phase. It was observed that TBR values in Phase II are much lower than those calculated in Phase I. Although direct comparison between Phases I and II are difficult, comparison between items within each phase is meaningful. Based on the higher TBR values for Phase I reinforced items, it could be suggested that placing the geosynthetic deeper in relatively thick airfield pavement sections reduces the realized benefit. A 16-in. maximum depth of placement was suggested by Tingle and Jersey [12] and Kinney et al. [13]. Tingle and Jersey [12] hypothesized that the performance benefit decrease could be attributed to reduced horizontal stress and/or deflection at increasing depth resulting in failure to fully mobilize the lateral restraint mechanism in the geosynthetics. Kinney et al. [13] found that the TBR decreased from a value in excess of 10 for base thicknesses of 10 in. or less to a value of 1 at base thicknesses of about 14 in. Al-Qadi et al. [14] found that for aggregate layer thicknesses ranging from 8 in. to 18 in., geogrid was effective in reducing horizontal shear deformation. They further concluded that for thicker base layers, optimal geogrid placement location was at the upper third of the layer, suggesting that performance benefit decreases with placement depth [14]. Robinson et al. [15] assembled data from test sections constructed with varying geogrid products in varying pavement structures over a range of loading conditions. It was concluded that performance improvement appeared to diminish with increasing depth of geogrid placement and approached no distinguishable improvement at a depth of approximately 22 in. [15].

Table 9. Difference in Control Item Properties for Phases I and II

Property	Control (Phase I)	Control (Phase II)	Difference (Phase I-Phase II)
CH Subgrade Properties			
Wet density (pcf)	110.3	111.2±1.2	-0.9
Dry density (pcf)	83.1	81.8±1.3	1.3
Nuclear moisture content (%)	32.7	36.0±1.2	-3.3
Oven-dried moisture (%)	35.4	38.2±0.9	-2.8
In-place CBR (%)	3.6	2.9±0.3	0.7
Thickness (in.)	27.8	27.8±0.1	0
P-154 Subbase Properties			
Wet density (pcf)	115.5	110.5±0.5	5
Dry density (pcf)	110.1	106.1±0.1	4
Nuclear moisture content (%)	4.9	4.1±0.4	0.8
Oven-dried moisture (%)	5.8	4.3±0.1	1.5
In-place CBR (%)	15	18	-3
Thickness (in.)	12.2	12.1±0.1	0.1
Crushed Limestone Base Properties			
Wet density (pcf)	141.4	137.9±2.6	3.5
Dry density (pcf)	134.3	134.2±2.4	0.1
Nuclear moisture content (%)	5.3	2.8±0.2	2.5
Oven-dried moisture (%)	5.1	2.5±0.2	2.6
In-place CBR (%)	88	100+	-12
Thickness (in.)	7.1	6.8±0.1	0.3
HMA Properties			
Density (% of G_{mm})	91.2	94.5	-3.3
Thickness (in.)	4.8	5.3±0.1	-0.5

Table 10. Comparison of Cycles-to-Failure and TBR

Test Item	Cycles at 1-in. Permanent Deformation		Cycles at 2-in. Permanent Deformation		TBR at 1-in. Permanent Deformation		TBR at 2-in. Permanent Deformation	
	Phase I	Phase II	Phase I	Phase II	Phase I	Phase II	Phase I	Phase II
Control	304	3,700	1,278	16,990	-	-	-	-
BX1200	6,322	9,720	25,960	44,960	20.8	2.6	20.3	2.6
TX140	1,000	1,460	4,304	9,890	3.3	0.4	3.4	0.6
Fornit 30/30	9,024	-	34,901	-	29.7	-	27.3	-
Fornit 40/40-25T	-	4,100	-	17,600	-	1.1	-	1.0
RS580*i*	-	2,575	-	20,830	-	0.7	-	1.2

Comparison in EPC responses in the top of subbase, top of subgrade, and bottom of subgrade at 1-in. and 2-in. permanent deformation are presented in tables 11 and 12, respectively. It was observed that measured EPC response values at 1-in. deformation were generally lower in Phase II than in Phase I for items where direct comparison was available. Reduced pressures throughout the pavement system support the hypothesis that differing asphalt properties may have influenced pavement performance.

Table 11. Comparison of Vertical Pressure Cell Response at 1-in. Permanent Deformation

Test Item	Top of Subbase (psi)		Top of Subgrade (psi)		Bottom of Subgrade (psi)	
	Phase I	Phase II	Phase I	Phase II	Phase I	Phase II
Control	53	35	18	14	13	4
BX1200	51	32	24	8	7	2
TX140	57	41	24	12	7	8
Fornit 30/30	44	-	44	-	14	-
Fornit 40/40-25T	-	46	-	16	-	7
RS580*i*	-	37	-	10	-	4

Table 12. Comparison of Vertical Pressure Cell Response at 2-in. Permanent Deformation

Item	Top of Subbase (psi)		Top of Subgrade (psi)		Bottom of Subgrade (psi)	
	Phase I	Phase II	Phase I	Phase II	Phase I	Phase II
Control	55	46	19	19	16	7
BX1200	57	59	26	20	9	8
TX140	59	44	26	16	8	9
Fornit 30/30	54	-	21	-	15	-
Fornit 40/40-25T	-	61	-	23	-	8
RS580*i*	-	58	-	19	-	7

8. CONCLUSIONS AND RECOMMENDATIONS.

Based on the test results in this report and comparisons to previous cyclic plate load tests completed for the Federal Aviation Administration (FAA), the following conclusions can be made:

- The inclusion of geosynthetics in airfield pavements, tested in medium-scale cyclic plate loading, display a performance benefit evidenced by increased cycles-to-failure and traffic benefit ratio (TBR) values greater than one when compared to an unreinforced control pavement.

- Data suggest that placing a geosynthetic deeper in a relatively thick airfield pavement may reduce the potential performance benefit.

- Some level of permanent deformation may be required to engage the reinforcing benefit of geotextiles, as suggested by higher TBRs at higher deformation values. This is consistent with the hypothesis that the primary reinforcement mechanism for geotextiles is tensioned membrane effect.

- The geosynthetics did not provide the same performance benefit as incorporating a subbase with 50+ California bearing ratio (CBR) in the pavement system. The intrinsic strength of the FAA P-154 subbase material essentially produced performance similar to additional base thickness.

- Changing the subbase material type and consequently CBR from approximately 20 to greater than 50 resulted in significant performance improvement.

Recommendations are as follows:

- Vertically applied load on a circular plate may produce different pavement response when compared to a rolling wheel load and/or wheel interactions. It is recommended that full-scale accelerated pavement testing be conducted to validate the results of medium-scale testing.

- Additional research is recommended to investigate the effect of geosynthetic placement depth under airfield pavement loading conditions to include placement at mid-depth and one-third depth within each aggregate layer.

- Single geosynthetic placement locations were evaluated in each pavement layer, and it is recommended that the incorporation of multiple geosynthetic layers and combination geotextiles/geogrids be evaluated in future work.

- It is recommended to investigate aperture size versus aggregate size to gain insight into aperture/aggregate compatibility as small subbase size aggregate may be compatible with smaller aperture sizes.

9. REFERENCES.

1. American Association of State Highway and Transportation Officials (AASHTO), "Standard Practice for Geosynthetic Reinforcement of the Aggregate Base Course of Flexible Pavement Structures," AASHTO R 50-09, Washington, D.C., 2009.

2. American Society for Testing and Materials (ASTM) International, "Standard Test Methods for Liquid Limit, Plastic Limit, and Plasticity Index of Soils," ASTM D4318-17e1, West Conshohocken, Pennsylvania, June 1, 2017.

3. ASTM International, "Standard Practice for Classification of Soils for Engineering Purposes (Unified Soil Classification System)," ASTM D2487-17, West Conshohocken, Pennsylvania, December 15, 2017.

4. AASHTO, "Standard Specification for Classification of Soils and Soil-Aggregate Mixtures for Highway Construction Purposes," AASHTO M 145-91, Washington, D.C., 2012.

5. ASTM International, "Standard Test Methods for Laboratory Compaction Characteristics of Soil Using Modified Effort (56,000 ft-lbf/ft^3 (2,700 kN-m/m^3))," ASTM D1557-12e1, West Conshohocken, Pennsylvania, May 1, 2012.

6. ASTM International, "Standard Test Method for California Bearing Ratio (CBR) of Laboratory-Compacted Soils," ASTM D1883-16, West Conshohocken, Pennsylvania, March 1, 2016.

7. Norwood, G.J., "Cyclic Plate Testing of Geogrid-Reinforced Airport Pavements—Phase I," Federal Aviation Administration report DOT/FAA/TC-19/xx, January 2019.

8. ASTM International, "Standard Test Methods for In-Place Density and Water Content of Soil and Soil-Aggregate by Nuclear Methods (Shallow Depth)," ASTM D6938-17a, West Conshohocken, Pennsylvania, November 1, 2017.

9. ASTM International, "Standard Test Methods for CBR (California Bearing Ratio) of Soils in Place," ASTM D4429-09a, West Conshohocken, Pennsylvania, December 1, 2009.

10. ASTM International, "Standard Test Method for Use of the Dynamic Cone Penetrometer in Shallow Pavement Applications," ASTM D6951/D6951M-09(2015), West Conshohocken, Pennsylvania, May 1, 2015.

11. AASHTO, "Standard Method of Test for Bulk Specific Gravity (G_{mb}) of Compacted Hot Mix Asphalt (HMA) Using Saturated Surface-Dry Specimens," AASHTO T 166, Washington, DC, January 2016.

12. Tingle, J., and Jersey, S., "Cyclic Plate Load Testing of Geosynthetic-Reinforced Unbound Aggregate Roads," *Transportation Research Record: Journal of the Transportation Research Board*, Transportation Research Board of the National Academies, Washington D.C., Vol. 1936, 2005, pp. 60-69.

13. Kinney, T., Abbott, J, and Schuler, J., "Benefits of Using Geogrids for Base Reinforcement with Regard to Rutting," *Transportation Research Record: Journal of the Transportation Research Board*, Transportation Research Board of the National Academies, Washington D.C., Vol. 1611, 1998, pp. 86-96.

14. Al-Qadi, I.L., Dessouky, S.H., Kwon, J., and Tutumluer, E., "Geogrid-Reinforced Low-Volume Flexible Pavements: Pavement Response and Geogrid Optimal Location," *Journal of Transportation Engineering*, Vol. 138, No. 9, 2012, pp. 1083-1090.

15. Robinson. W.J., Tingle, J.S., Norwood, G.J., and Howard, I.L, "Assessment of Equivalent Thickness Design Principles for Geosynthetic Reinforced Pavements by Way of Accelerated Testing," *Transportation Research Board 97th Annual Meeting*, Paper No. 18-01497, Washington, D.C., January 7-11, 2018.